Excitations and Magnetic Properties of Rare-Earth Al2 Compounds

Bak, Per

Publication date:
1974

Document Version
Publisher's PDF, also known as Version of record

Risø Report No. 312

Risø Report No. 312

Danish Atomic Energy Commission

Research Establishment Risø

Excitations and Magnetic Properties of Rare-Earth Al_2 Compounds

by Per Bak

July 1974

Sales distributors: Jul. Gjellerup, 87, Sølvgade, DK-1307 Copenhagen K, Denmark

Available on exchange from: Library, Danish Atomic Energy Commission, Risø, DK-4000 Roskilde, Denmark

July 1974

Risø Report No. 312

EXCITATIONS AND MAGNETIC PROPERTIES OF RARE-EARTH Al_2 COMPOUNDS

by

Per Bak

Danish Atomic Energy Commission

Research Establishment Risø

Physics Department

Abstract

Magnetic excitation spectra, measured by inelastic neutron scattering, and single-crystal magnetization curves of rare-earth Al_2 compounds are analysed using a Hamiltonian including 4th and 6th order crystal field terms and an isotropic exchange interaction between the magnetic ions.

The magnetic excitations - "excitons" - are transitions between single-ion atomic levels propagating through the lattice via the exchange interaction. In $NdAl_2$ dispersion relations of excited mean-field states are described for the first time. A double peak structure in the neutron spectrum of $TbAl_2$ is interpreted as a new effect: the magnon- exciton interaction. To calculate the excitation energies a Green's function theory was evaluated.

A detailed microscopic description of the magnetic anisotropy of $NdAl_2$, $PrAl_2$, $TbAl_2$, and $ErAl_2$ is given in terms of two temperature and field independent crystal field parameters by means of a two-dimensional mean-field theory. The crystal field parameters are shown to behave systematically throughout the entire rare earth Al_2 series, indicating that the effective charge distribution around the magnetic ions is independent of the particular rare earth constituent.

This report is submitted to the Technical University, Lyngby, in partial fulfilment of the requirements for obtaining the Ph. D (lic. tech) degree.

UDC 546.65 : 538.22

ISBN 87 550 0275 7

CONTENTS

1. INTRODUCTION

Magnetic properties of the $REAl_2$ (RE = Rare Earth) intermetallic compounds have been studied intensively during the last ten years. Of all the rare earth intermetallics they have received the greatest attention. All of the lanthanides combine with aluminum to form this compound. The structure is the so-called cubic Laves phase structure (figure 1), named after the Swiss crystallographer,who performed work on the prototype compound $MgCu_2$. However, the existence of the entire $REAl_2$ series was not established until two decades later in the work of Wernick and Geller[1]. Magnetization[2,3], and neutron diffraction measurements[4,5,6] verified that the compounds order magnetically and, with the exception of $TuAl_2$ and $CeAl_2$, form ferromagnets. The essential magnetic properties are given in table 1. Measurements of the paramagnetic ^{27}Al Knight shift[7] led to useful information about the conduction electron polarization[8].

The $REAl_2$ compounds are particularly well suited for both theoretical calculations and experiments. The local symmetry of the magnetic RE^{3+} ions is cubic, which simplifies the analyses

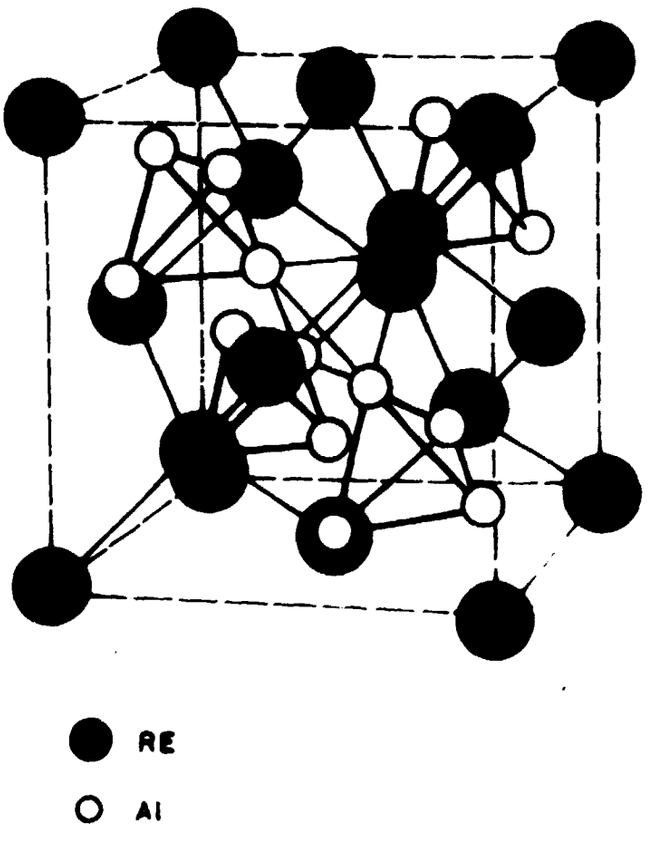

Fig. 1. The $REAl_2$ unit cell ($MgCu_2$ structure).

Table 1

Magnetic characteristics of $REAl_2$ compounds

Compound	Free ion ground state	gJ	Type	$M_o(\mu_B)$	$T_C(K)$	References
$CeAl_2$	$^2F_{5/2}$	2.14	antif.		3	10)
$PrAl_2$	$^3H_4$	3.20	ferro	2.62, 2.94, 2.88	34	10, 5, 6)
$NdAl_2$	$^4I_{9/2}$	3.28	ferro	2.27, 2.5	65, 77	10, 4, 9)
$TbAl_2$	$^7F_6$	9.00	ferro	8.6, 8.95	121, 105	10, 11)
$ErAl_2$	$^4I_{15/2}$	9.00	ferro	8.3, 8.8, 7.6	14	10, 5, 12)

greatly as will be shown in chapter 2. Furthermore large single crystals are available. This gives the opportunity of studying a series of closely related isostructural compounds which differ only in the nature of the rare earth constituent. We are thus able to extract information about the interactions between the magnetic 4f shell and the neighbouring ions.

This report presents an analysis of experiments carried out on single crystals of $REAl_2$ compounds. The analysis includes magnetic excitations measured by means of inelastic neutron scattering on $TbAl_2$ and $NdAl_2$, high field magnetization measurements on $PrAl_2$, $TbAl_2$, $NdAl_2$, and $ErAl_2$, and the magnetic heat capacity of $NdAl_2$ and $PrAl_2$. It is not intended to present a complete compilation of the magnetic properties of the $REAl_2$ compounds, although work of other authors will be mentioned to compare with the present analysis.

The following chapter gives a brief description of the interactions experienced by the rare earth ion as a result of its surroundings in the crystal. In chapter 3 we interpret neutron scattering measurements of the magnetic excitations. The experiments were carried out at Risø. The analysis of the exciton modes is carried out using a temperature-dependent Green's function technique in the random phase approximation. The theory, which involves operators creating transitions between mean-field or crystal field levels, is described in appendix A. A double-peak structure in the excitation spectrum of $TbAl_2$ is interpreted as a new resonance effect: the magnon-exciton interaction. The neutron spectrum of $NdAl_2$ consists of several branches. Dispersion relations of excited mean-field states are described for the first time. Chapter 4 is devoted to the bulk magnetic properties, such as magnetization curves at various temperatures and the magnetic specific heat. A microscopic description of the magnetic anisotropy is given in terms of two temperature and field independent crystal field parameters. The calculations are carried out using a two-dimensional mean-field theory. The combined λ-Schottky anomaly observed in $PrAl_2$ and $NdAl_2$ [9] is explained. Finally the results are summarized and discussed in chapter 5. It is shown that the crystal field parameters for the various compounds follow a systematic behaviour throughout the entire $REAl_2$ series, indicating that the effective charge distributions around the magnetic ions are independent of the particular rare earth constituent.

Most of the material in this work has been published previously in collaboration with H.-G. Purwins, J.G. Houmann, E. Walker, B. Barbara and M.F. Rossignol. For a more extensive treatment of the subjects in this report the reader is referred to the original articles.

2. CRYSTAL FIELD AND EXCHANGE INTERACTIONS

The magnetic properties of the rare earth compounds are determined by the combined effects of the magnetic interactions between the rare earth ions and the influence on the magnetic ions from the local surroundings in the lattice, the crystal field interaction. Experiments show, as will be evident in the chapters to follow, that these two effects are of the same order of magnitude for the $REAl_2$ compounds. In this chapter we shall briefly discuss the fundamental interactions and set up a simple model-Hamiltonian, which we shall use both to describe the bulk magnetic properties and the magnetic excitations.

2.1. Crystal Field Interactions

The ground state of the free rare earth ions is separated several thousands of degrees from the spin-orbit excited multiplets. The splittings due to crystal field end exchange interaction effects, when the ion is situated in the $REAl_2$ lattice, are much smaller. Hence we ignore the excited J-manyfolds and confine curselves to the ground state J-multiplet (see table 1).

For a rare earth ion with cubic surroundings the most general operator describing any single ion interaction inside a manyfold of given J is

$$\mathcal{H}_{cr} = B_4(O_4^0 + 5\,O_4^4) + B_6(O_6^0 - 21\,O_6^4) \qquad (2.1)$$

O_ℓ^m are Stevens operators as given by Abragam and Bleaney[13]. B_4 and B_6 are crystal field parameters. One may think of this Hamiltonian as describing the Coulomb interaction with the electrostatic charges set up by the ions in the environment. The number of parameters is reduced to two as a result of the high symmetry. This is the great advantage of working with compounds with cubi symmetry around the magnetic ions. The Hamiltonian gives rise to a

splitting of the groud state multiplet as described for example by Lea, Leask and Wolf[14]. The ions are distributed among the states according to Bolzmann statistics, the population of the states varying with temperature. These variations affect the magnetic and thermal properties significantly as will be shown in the ensuing chapters.

In the present work we deal with three fundamentally different rare earth systems:

1) $TbAl_2$: A singlet-triplet system,
2) $NdAl_2$: A Kramers doublet ground state system,
3) $PrAl_2$: A non-magnetic, orbital degenerate, doublet ground state system.

The crystal field level scheme may be determined directly by inelastic neutron scattering in the paramagnetic phase, provided the exchange interaction is comparatively low, or by measuring on diluted samples[15] such as $RE_xLa_{(1-x)}Al_2$. In this work the crystal field parameters are determined by analysing magnetic excitation spectra in the ordered temperature range and single -crystal magnetization curves.

2.2. Magnetic Interactions

The formation of magnetic structures implies the existence of magnetic interactions between the rare earth ions. The temperatures at which the magnetic ordering occurs for the $REAl_2$ compounds (table 1) exclude the possibility that the dipole interaction is dominant. Furthermore the rare earth sites are well separated. The overlap between orbitals centered on adjacent atoms therefore is very small or negligible, and hence direct exchange can be ruled out too. It is generally assumed that metallic rare earth systems can be represented by an assembly of magnetic RE -ions imbedded in a sea of conduction electrons. The particular mechanism involved is the indirect exchange interaction via the conduction electrons. The exchange interaction between the conduction electrons (s) and the 4-f electrons (S) may be written

$$\mathcal{H}_{sf} = \Gamma_{sf}\,\vec{S}\cdot\vec{s} \qquad (2.2)$$

where Γ_{sf} is the sf exchange integral. By means of this interaction

a rare earth ion with spin S sets up a long-range, oscillating spin density of the conduction electrons. A second magnetic ion couples to this spin density wave. This indirect coupling via the conduction electrons is referred to as the RKKY interaction[16,17]. The strength of the coupling depends on the amplitude and sign of the spin density at the second magnetic ion. To a first order approximation, using the free electron model of the conduction electrons, the effective coupling between ions i and j may be written as an isotropic Heisenberg exchange interaction term:

$$\mathcal{H}_{ex} = I(\vec{r}_i - \vec{r}_j)\, \vec{S}_i \cdot \vec{S}_j \qquad (2.3)$$

Within the ground state multiplet the spin can be projected on to the angular momentum:

$$\mathcal{H}_{ex} = \mathcal{J}(\vec{r}_i - \vec{r}_j)\, \vec{J}_i \cdot \vec{J}_j \qquad (2.4)$$

where

$$\mathcal{J}(\vec{r}_i - \vec{r}_j) = (g-1)^2\ I(\vec{r}_i - \vec{r}_j)$$

and g is the Landé factor.

Jaccarino et al.[7] have been able to determine both the magnitude and signs of the conduction electron polarization at the rare earth site in a number of the Al_2-compounds using nuclear and paramagnetic resonance technique.

The NMR measurements[7,19], together with analysis of Curie temperatures and magnetization of ternary $RE_x(Y,La)_{(1-x)}Al_2$ compounds[8], provide substantial support for the RKKY coupling mechanism. However, recent measurements[18] indicate the existence of a small anisotropic s-f interaction.

3. MAGNETIC EXCITATIONS IN $TbAl_2$ AND $NdAl_2$

The spontaneous magnetic moments of most of the $ReAl_2$ compounds are in general lower than the free ion moments (table 1). The crystal field is thus strong enough to produce considerable quenching, and therefore it is expected also to have strong effects on the magnetic excitation spectra. In particular we expect large

crystal field effects in the compounds $NdAl_2$ and $PrAl_2$ where the moment reduction is comparatively large. The magnetic excitations - "excitons" - in such systems are transitions between crystal field or mean-field single-ion levels, propagating through the lattice via the exchange interaction between the magnetic ions. Above the Curie temperature the excitations are essentially transitions between the Stark-split crystal field levels of the ground state J-multiplet with dispersion due to the exchange interaction. Below T_c the excitations can be described as transitions between combined crystal field and mean-field levels.

The dispersion relations for these excitations can in principle be measured by inelastic neutron scattering. For the compounds (such as $PrAl_2$ and $NdAl_2$) where crystal field and exchange energies are comparable, an analysis of the exciton spectra may yield both the crystal field parameters describing the local interactions on the magnetic ions from the cubic surroundings, and the wavevector dependence of the exchange interaction between the rare earth ions. In the other compounds (such as $TbAl_2$), where the quenching is low and the Curie temperature T_c comparatively high, simple spinwaves with an energy-gap (for $q = 0$) due to the crystal field and anisotropic exchange interaction are expected. Previous neutron diffraction measurements of the low temperature magnetic excitations in $TbAl_2$ confirm this picture[20]. In this case a determination of the crystal-field parameters from the dispersion curves is difficult. A more precise determination can be obtained from single crystal magnetization curves (see section 4), or from inelastic neutron scattering on diluted samples[15].

Appendix A presents a Green's function theory for the magnetic excitons in a system with arbitrary crystal field levels and two -ion interactions. In the low-temperature limit the theory includes the usual spinwave theory and Grover's theory[21] for magnetic excitons.

In section 3.2 the theory is used to interpret the temperature dependence of the exciton spectrum of $TbAl_2$. At elevated temperatures inelastic neutron scattering measurements show a double peak structure in the scattered neutron intensity. This splitting of the spinwave branch is interpreted as an interaction between the spinwaves and the excitations associated with higher

lying magnetic states, a "magnon-exciton interaction". This is the first observation and theoretical interpretation of an interaction of this kind. In 3.1 the exciton spectrum of $NdAl_2$ is analysed. This is the first analysis of the magnetic excitation spectrum in a rare earth ferromagnet showing dispersion of excited mean-field levels.

3.1. Dispersion Relations for Magnetic Excitons in $NdAl_2$

$NdAl_2$ is an example of a magnetic system in which the crystal field and exchange energies are of the same order of magnitude. The easy and hard directions of magnetization are <100> and <111> respectively[18] and the spontaneous magnetic moment at 4.2 K is $2.5 \pm 0.1\ \mu_B$[4] compared to the free ion value $3.27\ \mu_B$ of the $^4I_{9/2}$ multiplet of the Nd^{3+} ion.

The magnetic excitation spectrum at 5 K was measured at Risø by means of inelastic neutron scattering[31]. The measurements were performed on a triple axis spectrometer at the DR 3 reactor at Risø using a large single crystal of $NdAl_2$ produced by the Czochralski method[22]. This allowed us to determine the dispersion relations for the magnetic exciton branches over the whole Brillouin zone. We were thus not restricted to measuring spherically averaged dispersion relations as was the case for previous measurements on powder samples of rare earth compounds. The measurements were carried out around the [1 1 1] [2 0 0] and [2 2 0] reciprocal lattice points for momentum transfer in the <110> direction.

In $NdAl_2$ there are two magnetic ions per unit cell, so that the excitation spectrum can be separated into optical and acoustic branches (appendix A). For momentum transfer in the <110> direction the magnetic structure factor is $(1 \pm \cos(\vec{\tau}\cdot\vec{\rho}))$, where $\vec{\tau}$ is the reciprocal lattice vector and $\vec{\rho}$ is the vector joining an ion in one sublattice to its nearest neighbour in the other sublattice. For $NdAl_2$ $\vec{\rho} = a \times (\frac{1}{4}\ \frac{1}{4}\ \frac{1}{4})$. The plus and minus signs are valid for the acoustic and optical modes respectively. For $\vec{\tau} = \frac{2\pi}{a} \times [2\ 2\ 0]$ the optical modes therefore have zero structure factor whereas the acoustic modes are unobservable for $\vec{\tau} = \frac{2\pi}{a} \times [2\ 0\ 0]$. Around [1 1 1] the two structure factors are equal. We are thereby able to distinguish between optical and acoustic modes. The experimental results are given in fig. 2. Two well-resolved low-lying excitation branches were observed, one acoustic and one optical. It was

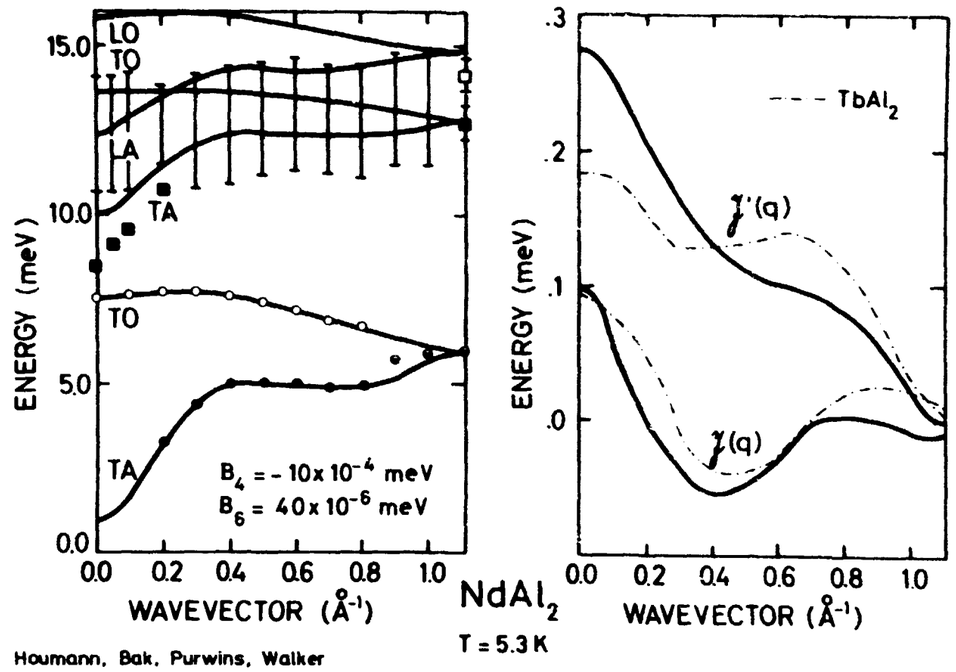

Fig. 2. (a) Dispersion relations for magnetic excitons in $NdAl_2$ for momentum transfer in the <110> direction. The full lines are a theoretical fit to the experimental results obtained as explained in the text. (b) The form of $\mathcal{J}(\vec{q})$ and $\mathcal{J}'(\vec{q})$ in the <110> direction deduced from the fit. Broken line: corresponding curves for $TbAl_2$. TO: Transverse optical branches; TA: Transverse acoustic branches; LO: Longitudinal optical branch; LA: Longitudinal acoustic branch.

not possible to resolve the acoustic branch below $q = 0.2\ Å^{-1}$. At higher energies we observed a band of scattered neutron intensity which is completely resolved into two peaks only near the zone boundary. Near the zone centre we could resolve one acoustic branch, whereas no optical branch could be observed in this energy region for instrumental reasons. The existence of three well-defined excitations at the zone boundary, where the optical and acoustic modes are degenerate, implies six exciton modes for a general point of the Brillouin zone.

The Hamiltonian for the Nd ions is written as the sum of crystalline electric field and isotropic Heisenberg exchange interaction terms. Regrouping these terms into a single-ion term $\mathcal{H}_1$ including the crystal field and the molecular field part of the exchange term, and a two-ion term $\mathcal{H}_2$ we obtain

$$\mathcal{H} = \mathcal{H}_1 + \mathcal{H}_2 \qquad (3.1)$$

where

$$\mathcal{H}_1 = \sum_i \left(B_4(O^0_{4i} + 5\,O^4_{4i}) + B_6(O^0_{6i} - 21\,O^4_{6i})\right.$$
$$\left. - 2(\mathcal{J}(\vec{q}=0) + \mathcal{J}'(\vec{q}=0))\langle J^z\rangle J^z_i\right)$$
$$+ N(\mathcal{J}(\vec{q}=0) + \mathcal{J}'(\vec{q}=0))\langle J^z\rangle^2 \qquad (3.2)$$

$$\mathcal{H}_2 = \sum_{ij} \mathcal{J}_{ij}\,\vec{J}_i\cdot\vec{J}_j, \quad \vec{J}_i = \vec{J}_i - \langle J^z\rangle\,\vec{\epsilon}_z \qquad (3.3)$$

The quantization axis has been chosen along the easy direction (<100>). $\mathcal{J}(\vec{q})$ and $\mathcal{J}'(\vec{q})$ are respectively the Fourier transforms of the exchangeinteraction $\mathcal{J}_{ij}$ within one sublattice and between the two sublattices. $\vec{\epsilon}_z$ is a unit vector along this direction. The analysis of the excitation spectrum proceeds as follows.

For a number of different values for B_4 and B_6 the single ion,crystal-field-only isothermal susceptibility $\chi_o(T)$ is calculated at the Curie temperature 65 K by means of equation (4.17). At this temperature the inverse susceptibility $1/\chi(T)$ approaches zero. Using the formula

$$1/\chi(T) = 1/\chi_c(T) - \frac{2(\mathcal{J}(0) + \mathcal{J}'(0))}{g^2\,\mu_B^2} \qquad (3.4)$$

the mean-field constant $2(\mathcal{J}(0) + \mathcal{J}'(0))$ is chosen such that the theoretical transition temperature is in agreement with experiment. As the next step, $\mathcal{H}_1$ is diagonalized self-consistently as a function of temperature to deduce the molecular field, H_{MF}, the single ion wavefunctions, $|n\rangle$,and the energy levels E_n. The excitation spectrum is calculated in the RPA-approximation, taking into account all 10 single ion levels using the theory presented in appendix A. The energies are the roots of the characteristic determinant (A.18). For the acoustic branches, $\mathcal{J}(\vec{q})$ is replaced by $\mathcal{J}(\vec{q}) + |\mathcal{J}'(\vec{q})|$ and for the optical branches $\mathcal{J}(\vec{q})$ is replaced by $\mathcal{J}(\vec{q}) - |\mathcal{J}'(\vec{q})|$. The magnetic structure factor $(1 \pm \cos(\vec{\tau}\cdot\vec{\rho}+\phi))$ must be taken into account in this case. ϕ is a phase angle determined by $\mathcal{J}'(\vec{q}) = |\mathcal{J}'(\vec{q})|\exp(i\phi)$. For $\vec{q}$ in the <110> direction, ϕ is equal to zero. For rare earth ions in a cubic environment, at least two of the matrix elements $\langle n|J^+|m\rangle$, $\langle n|J^-|m\rangle$, and $\langle n|J^z|m\rangle$ are zero. This means that the equations (A.18) determining the exciton dispersion relations can be separated into two

set of equations. One set involves matrix elements of J^+ and J^- only. The excitation branches determined by this part of the linear system of equations are denoted transverse. The other set of equations, involving matrix elements of J^z only, determines the longitudinal excitations. At zero temperature this approach is equivalent to the pseudo-Boson method introduced by Grover[21], and the many level spinwave theory of Buyers et al.[23] used to interpret the exciton spectrum of TbSb[24].

The neutron scattering cross section is proportional to the imaginary part of the dynamic susceptibility[25]

$$\frac{d^2\sigma}{d\Omega d\omega}(\vec{q},\omega) \sim \left(1-\exp(-\omega/kT)\right)^{-1}\,\mathrm{Im}\left(\chi^{zz}(\vec{q},\omega) + \tfrac{1}{2}(\chi^{+-}(\vec{q},\omega)+\chi^{-+}(\vec{q},\omega))\right) \qquad (3.5)$$

From eq. (A.21) it is readily seen that the poles of the longitudinal susceptibility $\chi^{zz}(\vec{q},\omega)$, and the transverse susceptibility, $\frac{1}{2}(\chi^{+-}(\vec{q},\omega) + \chi^{-+}(\vec{q},\omega))$,are the longitudinal and transverse excitation energies, respectively. The intensities can thus be calculated from the residues of the dynamic susceptibility, which can be calculated as a sum of Green's functions (A.21), or directly from (A.22). The Fourier transformed exchange interaction $\mathcal{J}(\vec{q}) \pm \mathcal{J}'(\vec{q})$ is determined for $\vec{q} \neq \vec{0}$ by fitting the calculated dispersion relations to the two low-lying branches. By an iteration process B_4 and B_6 are determined as the parameters giving the best agreement with the upper branches. We find:

$$B_4 = -1.0 \times 10^{-3}\ \text{meV}, \quad B_6 = 4.0 \times 10^{-5}\ \text{meV}$$

$\mathcal{J}(\vec{q})$ and $\mathcal{J}'(\vec{q})$ are given in figure 2b. Figure 3 shows the single-ion level scheme as a function of the internal molecular field. The crystal-field-only scheme has a doublet, Γ_6, as the ground state and two quartets, $\Gamma_8^{(1)}$ and $\Gamma_8^{(2)}$, as excited states. In the exchange field, the degeneracy of these states is lifted and the crystal field wavefunctions are mixed. The energies and the wavefunctions of the crystal field states and the mean-field states at 5 K are given in the diagrams in figures 18 and 19.

The mean-field states are denoted $|1\rangle$,$|2\rangle$.....$|10\rangle$ ordered according to increasing energy. The magnetic moment of the MF ground state $|1\rangle$ is 2.6 μ_B,in excellent agreement with the experimental value 2.5 ± 0.1 μ_B[4].

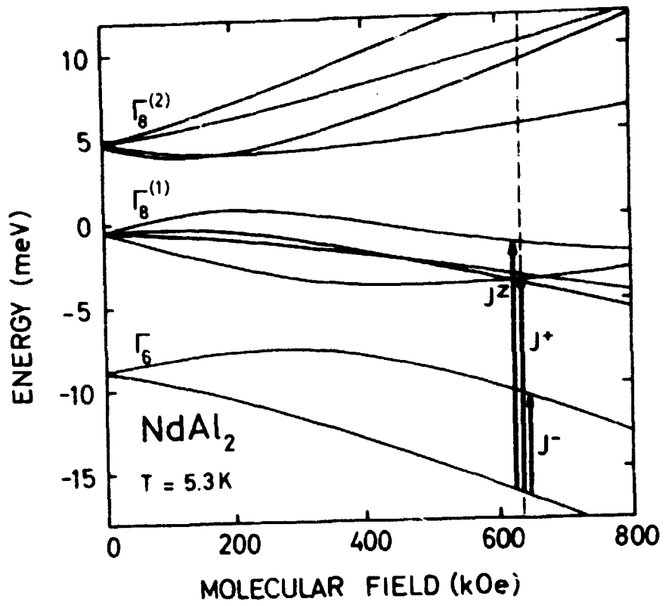

Fig. 3. Single-ion level scheme of $NdAl_2$ as a function of molecular field. The vertical line indicates the actual molecular field 630 kOe obtained by the self-consistent diagonalization of $\mathcal{H}_1$.

The most important matrix elements creating excitations between the levels at low temperatures are

$$\langle 2|J^-|1\rangle = 3.25$$
$$\langle 5|J^+|1\rangle = 2.28$$
$$\langle 6|J^z|1\rangle = -1.71$$

The first two matrix elements give rise to two optical and two acoustic transverse modes. The last matrix element creates two longitudinal branches. Corresponding acoustic and optical branches are degenerate at the zone boundary due to symmetry. The calculated dispersion relations are shown as solid lines in figure 2a.

The two lowest excitation branches are of transverse type originating mainly from the matrix element $\langle 2|J^-|1\rangle$ between the ground state, $|1\rangle$, and the other state, $|2\rangle$, associated with the doublet crystal field state. Since the corresponding wavefunctions are approximately $|J,J-1\rangle$ and $|J,J\rangle$ these branches correspond to ordinary spin waves in magnetic systems with strong single ion anisotropy. The remaining four exciton branches of transverse and

longitudinal character are associated with transitions between the ground state and excited states originating from the $\Gamma_8^{(1)}$ quartet. Matrix elements between the ground state and the higher states are much smaller, and consequently the excitations associated with these states could not be observed in the experiment. The qualitative features of the exciton spectrum are only slightly dependent on the crystal field parameters. For essentially all reasonable values of B_4 and B_6 the theoretical spectrum consists of six strong modes. To our knowledge this is the first time that excited mean-field states have been observed. The excitons seem to be rather well defined, especially around $\vec{q} = 0$ and the zone boundary. Near the zone centre, dispersion of the mean field levels is clearly demonstrated. The present analysis shows that the effective Weiss-field is not merely an artificial phenomenological device to explain magnetic ordering, but indeed acts as a real magnetic field, creating observable single-ion levels. The deviations from the mean-field theory just give rise to a relatively small q-dependence of the energy.

The magnetic excitation spectrum of $NdAl_2$ at 5.3 K can thus be well understood using a Hamiltonian including crystal field and isotropic exchange interaction terms. In view of the simplicity of the Hamiltonian (anisotropic exchange and magnetoelastic effects are neglected) the agreement between experiment and theory is remarkably good. However, further measurements are planned to obtain more detailed experimental information. In particular one may hope to be able to measure the dispersion of the pure crystal field transitions in the paramagnetic regime and thus determine the crystal field and exchange parameters in an independent way. Furthermore a better resolution of the upper exciton branches should be possible. In chapter 4 it will be shown that magnetization measurements provide strong support for the crystal field parameters extracted from the exciton dispersion curves.

The Fourier transformed exchange interactions, $\mathcal{J}(\vec{q})$ and $\mathcal{J}'(\vec{q})$ are shown together with the corresponding values for $TbAl_2$ determined from ordinary spinwave dispersion curves[20] in figure 2. The similarity between the interactions in the two compounds is rather striking. Assuming simple RKKY exchange interaction between the magnetic ions one should expect $\mathcal{J}(\vec{q})$ and $\mathcal{J}'(\vec{q})$ to be

proportional to the de Gennes factor $(g-1)^2$. For Nd^{3+} and Tb^{3+} one finds

$$\frac{(g_{Tb} - 1)^2}{(g_{Nd} - 1)^2} = 3.36 >> 1 \qquad (3.6)$$

The similarity between both the shapes and the magnitudes of the curves implies that the interaction between the magnetic ions acts effectively as an $\vec{J}\cdot\vec{J}$ interaction rather than the $\vec{S}\cdot\vec{S}$ interaction given by the RKKY theory. Hence there is no doubt that orbital contributions to the exchange interaction are important[26].

3.2. Magnon-exciton interaction in $TbAl_2$

It has been pointed out[27] that in the paramagnetic region magnetic excitations from the ground state of a lattice of rare earth ions can interact with excitations between excited magnetic states with very low population, provided that the energies of the non-interacting excitations are comparable. This interaction leads to splittings of the magnetic exciton branches which can in principle be observed by inelastic neutron scattering. In this section it is shown that a splitting of the same nature can occur also in the ordered phase. This is the first observation and theoretical interpretation of an interaction of this kind.

$TbAl_2$ orders ferromagnetically below 105 K[28]. The easy and hard directions of magnetization are <111> and <100> respectively and the magnetic moment observed from low-temperature magnetization measurements has the free ion value of 9 μ_B[11]. The Curie temperature is high compared with other $REAl_2$ compounds (table 1). Accordingly the quenching of the low temperature spontaneous magnetic moment is very small, and the magnetic excitations are ordinary spinwaves with an energy gap at $\vec{q} = 0$ due to crystal field effects. The magnon dispersion relations for both the acoustic and optical branches at 4.2 K have been reported recently[20]. However, we shall see that when the temperature is raised, the excitation spectrum behaves in a most unusual way.

To investigate the temperature dependence of the spinwaves an inelastic neutron scattering experiment was carried out by Houmann et al.[30]. The experiment was performed on a triple axis spectrometer at the DR 3 reactor at Risø. The constant q mode of operation was used. Some typical experimental results are shown

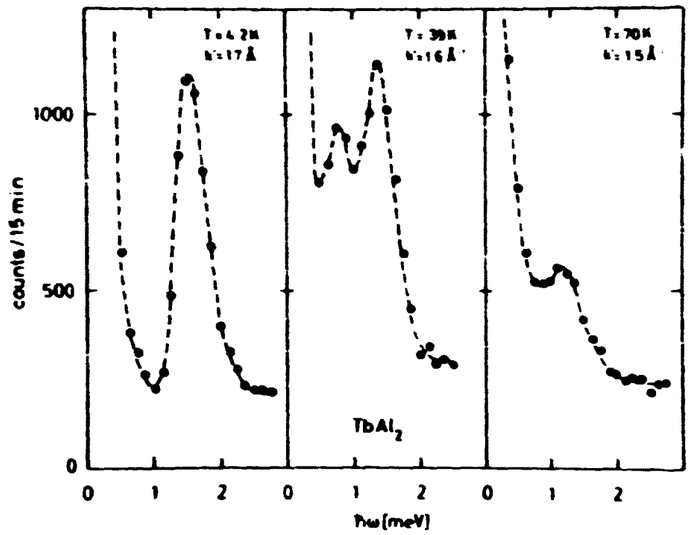

Fig. 4. Neutron intensity measured for $TbAl_2$ at the (111) reciprocal lattice point corresponding to q = 0. k' is the wave vector of the scattered neutrons and ħω the energy transfer from the neutrons.

in fig. 4. At 4.2 K a well-defined magnon peak at 1.58 meV is observed. As the temperature is raised to about 35 K, a new peak arises in the neutron spectrum with lower energy than the original magnon peak. The intensity of the new peak increases with increasing temperature while the intensity of the upper peak decreases. Above 60 K the low-energy peak, which has taken over most of the intensity, disappears into the background. Fig. 5 shows the experimental points for all measured wavevector transfers and temperatures. The striking feature of the experimental results is the observed splitting of the original magnon branch into two branches at elevated temperatures. The behaviour, that one would have anticipated, was a simple renormalization of the magnon energies following a simple power law[29]. We shall interpret this double peak structure as an interaction between the magnon modes and a magnetic exciton originating from a transition between some higher-lying excited magnetic states.

The strong interactions between the magnetic ions and the corresponding small quenching of the magnetic moment implies that the eigenfunctions of the magnetic ions are simple $|J,M_J\rangle$ states. The $J_i^- J_j^+$ part of the isotropic exchange interaction between the ions i and j has large matrix elements between neighbouring levels, whereas the matrix elements of J^z can be ignored. Only transverse

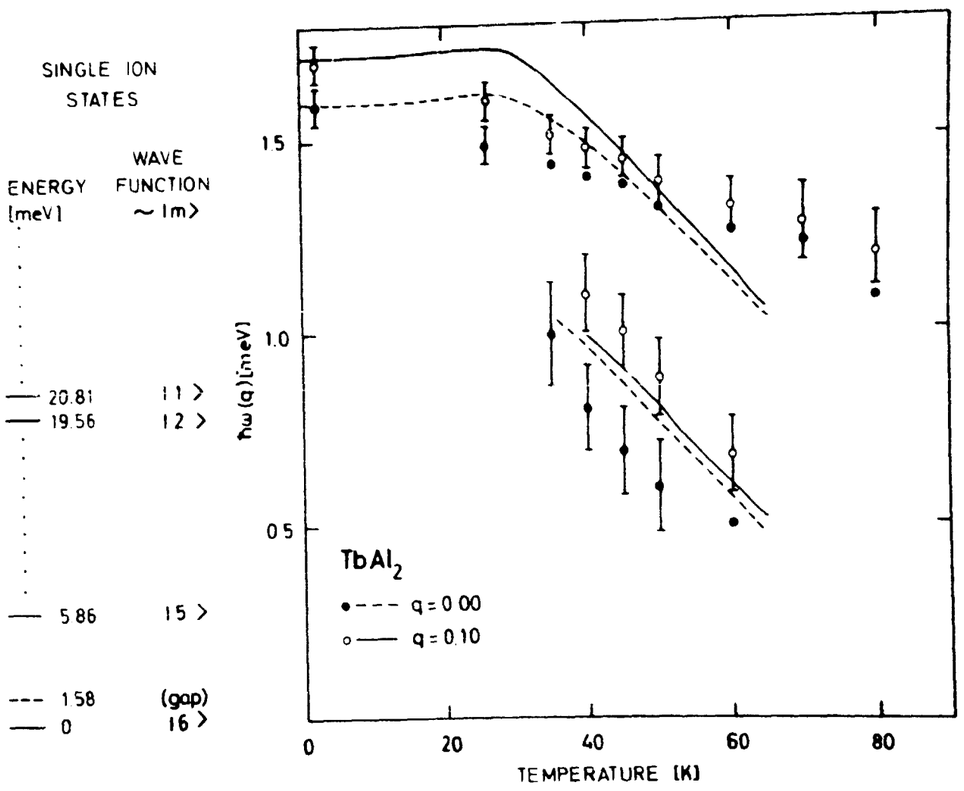

Fig. 5. Temperature dependence of the magnetic excitation energies in $TbAl_2$. Full and dotted lines: theory. Points: experiment. The left-hand side of the figure shows the single-ion states of Tb^{3+} at 4 K.

magnetic excitations (like spinwaves) are expected in this case. The crystal field part of the Hamiltonian acts as a perturbation shifting the mean-field levels without changing the wavefunctions substantially. The shift between the two lowest lying levels determines the energy gap associated with normal low-temperature spinwaves. In general the temperature dependence of the lowest excited levels combined with a change in population of the mean field levels gives rise to the temperature-renormalization of the spinwave energies and the energy gap. However, if the energy difference between two succeeding excited levels becomes comparable to the spinwave energy, the coupling between the corresponding excited state magnon (exciton) and the spinwaves via the two-ion matrix elements of the exchange interaction becomes important, i.e. an interaction between the modes takes place (see appendix 1). This resonance gives rise to a mixing of the magnon mode and the exciton mode and hence to the observed anti-crossing effects, analogous to the

magnon-phonon interaction, causing similar splittings of the magnon branches[32]. However, in the latter case, the phonon represents a transition from the Boson ground state of the lattice at low temperatures, and therefore the interaction can be observed even at 0 K. In the actual case the excited states corresponding to the exciton mode are not populated at low temperatures, and consequently there will be no interactions. However, when the temperature increases, the excited states become populated, and the interaction becomes possible. The temperature dependent population factors of the excited states prohibit a direct observation of the transitions between these states; the excited states can thus only be observed through the magnon-exciton interaction.

The qualitative physical picture described here can be confirmed quantitatively using the Green's function theory described in appendix A. The analysis, taking into account all 13 energy levels of the ground state J = 6 multiplet, involves only 3 parameters.

The Hamiltonian for the Tb ions is written as the sum of crystalline electric field and isotropic Heisenberg exchange terms. Regrouping these terms into a single ion term $\mathcal{H}_1$ and a two-ion term $\mathcal{H}_2$ we obtain

$$\mathcal{H} = \mathcal{H}_1 + \mathcal{H}_2 \tag{3.7}$$

where

$$\begin{aligned}\mathcal{H}_1 = \sum_i \Big[& -(2/3)\, B_4 \,(O^0_{4i} - 20\sqrt{2}\, O^3_{4i}) \\ & + (16/9)\, B_6 \,(O^0_{6i} + (35\sqrt{2}/4)\, O^3_{6i} + (77/8)\, O^6_{6i}) \\ & -2(\mathcal{J}(q=0) + \mathcal{J}'(q=0))\, \langle J_z \rangle\, J_{zi} \Big] \\ & + N(\mathcal{J}(q=0) + |\mathcal{J}'(q=0)|)\, \langle J_z \rangle^2,\end{aligned} \tag{3.8}$$

and

$$\mathcal{H}_2 = -\sum_{ij} \mathcal{J}_{ij}\, \vec{J}_i \cdot \vec{J}_i \qquad \vec{J}_i = \vec{J}_i - \langle J_z \rangle\, \vec{\epsilon}_z \tag{3.9}$$

The quantization axis (z-direction) is taken along the direction of magnetization (<111>).

$\mathcal{H}_1$ is diagonalized self-consistently as a function of temperature to yield mean-field eigenfunctions and energies to serve as a basis for calculating the exciton spectrum. The calculations are carried out for a wide range of crystal field parameters B_4 and B_6, and exchange constants $\mathcal{J}_{eff}(0) = \mathcal{J}(0) + \mathcal{J}'(0)$. However, it is not permissible to vary the parameters unrestricted to explain the magnon-exciton interaction. The macroscopic magnetic properties calculated on the basis of these parameters must be in agreement with the following experimental facts:

1) The easy direction of magnetization is the <111> direction[18].
2) The Curie temperature T_c is 105 K[28]. The mean-field transition temperature determined by $\mathcal{H}_1$ must correspond to this value.
3) The low temperature spontaneous magnetic moment is near to the free-ion value 9 μ_B[11].
4) The spinwave energy gap at 0 K is 1.6 meV.

These conditions impose severe restrictions on the parameters. In fact there is only very little freedom left to vary the parameters to explain the detailed behaviour of the excitation spectrum as a function of temperature.

The excitation energies are the roots of the secular determinant (A.18), including transitions between all 13 levels. The calculation is carried out for the acoustic modes determined by the sum of the Fourier transforms $\mathcal{J}(\vec{q})$ and $|\mathcal{J}'(\vec{q})|$ (section A.2). Matrix elements, weighed by the relevant population factors n_n, which are more than two orders of magnitude smaller than the matrix element between the two lowest states, are ignored. The best agreement with experiment was obtained using the parameters

$B_4 = 7.0 \times 10^{-4}$ meV

$B_6 = 2.15 \times 10^{-6}$ meV

$\mathcal{J}'(0) + \mathcal{J}(0) = 0.325$ meV

The mean-field energy levels at 50 K (H_{MF} = 417 kOe) are shown in the diagram below. The most important "diagonal elements" in the determinant of (A.18) correspond to the transitions marked by arrows.

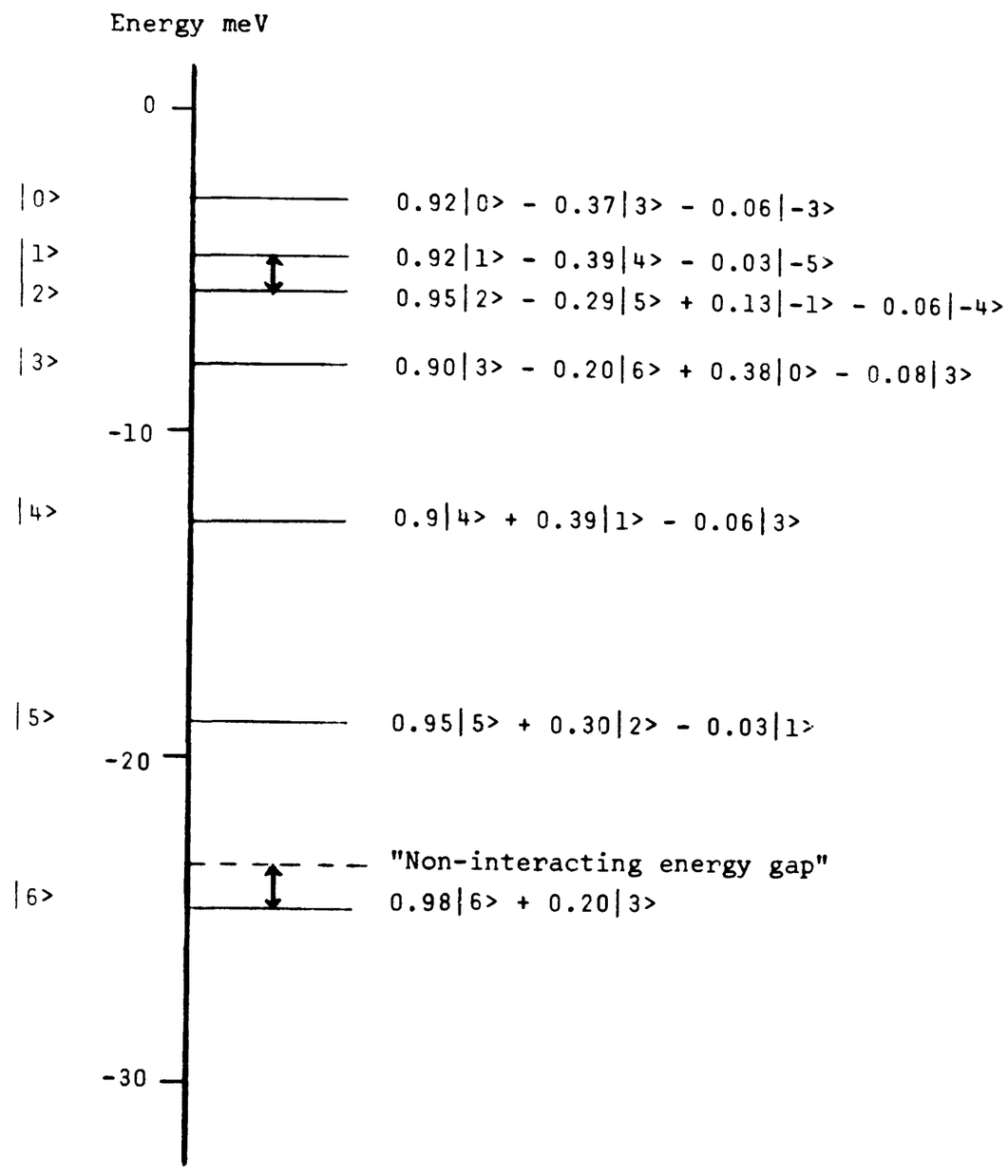

Mean field levels of $TbAl_2$ at 50 K

The inelastic neutron scattering cross section is proportional to the imaginary part of the dynamic susceptibility $\chi(\vec{q},\omega)$ (3.5). In the case of $TbAl_2$ we get ($\chi^{zz}(\vec{q},\omega) \sim 0$)

$$\frac{d^2\sigma}{d\Omega d\omega}(\vec{q},\omega) \sim \left(1-\exp(-\beta\omega)\right)^{-1} \mathrm{Im}\left(\chi^{+-}(\vec{q},\omega) + \chi^{-+}(\vec{q},\omega)\right) \qquad (3.10)$$

The dynamical susceptibilities are determined directly from the Green's functions (A.21). The calculated energies of the modes with measurable neutron cross sections are given in fig. 5, together with the single-ion level scheme at 0 K. The parameters used in the calculation give a molecular field transition temperature of 105 K and nearly pure J_z single ion states. We therefore denote these states by the corresponding J_z quantum number. B_4 and B_6 are of the same order of magnitude as the parameters used to describe the magnetization data for $TbAl_2$ (see section 4). They also give the correct easy and hard directions of magnetization. At low temperatures the calculation shows only one acoustic excitation branch. This can be interpreted as an ordinary magnon branch with an energy gap, since it is mainly due to a $|J> \rightarrow |J-1>$ transition. As the temperature is raised the upper states become slightly populated. The renormalized magnon energy approaches and crosses the energy difference between the excited states $|2>$ and $|1>$, so that an interaction between the $|2> \rightarrow |1>$ exciton and the magnon can take place. In the temperature range where the measurements were carried out, the population of the excited states corresponding to the exciton is very small. Consequently the neutron scattering cross section for the exciton is at least two orders of magnitude smaller than that for the magnon. The experimental ratios between the intensities of the low-lying and the high-lying excitation is roughly 1 to 4 at 35 K and 1 to 1 at 45 K, compared with the theoretical prediction of 1 to 5.2 and 1 to 1.3 respectively. At higher temperatures it was not possible to obtain a sufficiently accurate determination of the intensities to make such a comparison, however,it is obvious that the low-lying excitation is the most intense in agreement with theory. In view of the simplicity of the Hamiltonian used in the interpretation (magnetostriction and possible anisotropic exchange have been ignored) the agreement between theory and experiment is remarkably good.

We conclude that interactions between magnetic excitations may occur if the energies of two modes are comparable. This resonance gives rise to additional peaks in the excitation spectrum, which can be directly measured by inelastic neutron scattering. This effect shows up in $TbAl_2$ despite the fact that we are dealing with nearly pure J_z single ion states and that the excitations at low temperature can be described as ordinary magnons, with an energy gap due to the crystalline electric field. The effects that are observed in $TbAl_2$ may well occur in other rare earth substances and possibly explain certain discrepancies between experiments and the theory previously used to interpret them. It is planned to extend the measurements to larger q values.

4. MAGNETIZATION AND HEAT CAPACITY

The analysis of the magnetic excitation spectrum of $NdAl_2$ and $TbAl_2$ has given us detailed information about the fundamental microscopic magnetic interactions in the $REAl_2$ compounds. Another source of information is measurements of the bulk magnetic properties, such as the spontaneous magnetization below T_c, the magnetization in externally applied magnetic fields, the susceptibility, and the magnetic specific heat.

In this chapter, single crystal magnetization curves of $PrAl_2$, $TbAl_2$, and $ErAl_2$ will be analysed by means of a two-dimensional mean-field theory, and crystal field parameters will be derived. Furthermore we shall show that the magnetic properties of $NdAl_2$ can be understood using the crystal field parameters derived from the exciton spectrum in chapter 3. Finally theoretical heat capacities of $NdAl_2$ and $PrAl_2$ will be compared with experiment.

4.1. Two-Dimensional Mean-field Theory

As usual we assume that the single-ion part of the Hamiltonian can be written

$$\mathcal{H}_1 = B_4(O_4^0 + 5\,O_4^4) + B_6(O_6^0 - 21\,O_6^4) - g\mu_B(\vec{H}_e + \vec{H}_{MF})\cdot\vec{J} + \tfrac{1}{2}\lambda M^2 \qquad (4.1)$$

The mean field, $\vec{H}_{MF}$, obeys the self-consistency equation:

$$\vec{H}_{MF} = \lambda\vec{M} = g\mu_B\lambda \langle\vec{J}\rangle, \qquad \lambda = \frac{2(\mathcal{J}(o) + \mathcal{J}'(o))}{g^2\mu_B^2} \tag{4.2}$$

The coordinate axes have been chosen along the cube edges. A Zeeman term originating from an applied magnetic field, $\vec{H}_e$, has been included.

Let us first consider the case ($PrAl_2$ [33], $NdAl_2$ [35]), where the easy direction of magnetization is along the <100> direction. For an external magnetic field in this direction, the self-consistent diagonalization of $\mathcal{H}_1$ is carried out in the usual way [34]. The direction of the magnetic moment remains in the <100> direction. When the external magnetic field is applied along other symmetry directions, the analysis is more complicated. As the field increases from zero, the direction of the magnetic moment rotates from the <100> direction towards the direction of the magnetic field. At the same time the quenching of the magnetic moment changes. Thus, the absolute value of the magnetization vector, $|\vec{M}|$, changes even at 0 K. This is a pure quantum-mechanical effect which invalidates a semiclassical analysis treating $\vec{M}$ as a classical vector with constant length. Instead we introduce a two-dimensional mean-field theory. In the case where the external magnetic field is in the <110> direction (figure 9a) the effective magnetic fields may be written

$$H^z = \frac{H_e}{\sqrt{2}} + \lambda M^z \tag{4.3}$$

$$H^x = \frac{H_e}{\sqrt{2}} + \lambda M^x \tag{4.4}$$

$$M^\alpha = \left\{\sum_n \exp(-\frac{E_n}{kT})\right\}^{-1} \sum_n \langle n|M^\alpha|n\rangle \exp(-\frac{E_n}{kT}) \tag{4.5}$$

E_n is the energy of the n'th level. The magnetization along the external field is then

$$M^{<110>} = \frac{M^z}{\sqrt{2}} + \frac{M^x}{\sqrt{2}} \tag{4.6}$$

The magnetization curve, $M^{<110>}$ versus H_e, is calculated by diagonalizing (4.1) together with the two mean-field equations (4.3)

and (4.4) by an iteration process. A computer programme was written to carry out such calculations. The moment is implicitly assumed to be confined to the xz-plane. For an external magnetic field in the <111> direction the computations are facilitated by transforming the Hamiltonian into a coordinate system where the x-axis is in the <110> direction (figure 9b) to avoid diagonalizing complex matrices involving J^y. This is easily carried out by rotating the Hamiltonian 45° around the quantization axis (z-axis).

$$\mathcal{H}'_1 = B_4(O_4^0 - 5\,O_4^4) + B_6(O_6^0 + 21\,O_6^4) - g\mu_B(\vec{H}_{MF} + \vec{H}_e)\cdot\vec{J} \tag{4.7}$$

The self-consistency conditions are

$$H^z = \frac{H_e}{\sqrt{3}} + \lambda M^z \tag{4.8}$$

$$H^x = \frac{H_e\sqrt{2}}{\sqrt{3}} + \lambda M^x \tag{4.9}$$

$$M^{<111>} = \frac{M^x\sqrt{2}}{\sqrt{3}} + \frac{M^z}{\sqrt{3}} \tag{4.10}$$

In the case ($TbAl_2$, $ErAl_2$), where the easy direction is along the <111> direction, the calculations are most easily carried out in the coordinate system with the x-axis along a <110> direction, the corresponding Hamiltonian being (4.7). The xz-plane contains all the main symmetry directions (figure 9b). The corresponding mean-field equations are simply

$$H^z = H_e^z + \lambda M^z \tag{4.11}$$

$$H^x = H_e^x + \lambda M^x \tag{4.12}$$

H_e^x and H_e^z are determined by the directions of the applied magnetic field. Again the self-consistent diagonalization is carried out on a computer using an iteration method. The present procedure allows us to determine the detailed behaviour of the quantum-mechanical magnetization vector $\vec{M}$ in an external magnetic field. The magnetization curves can be calculated at all temperatures without introducing new phenomenological, temperature-dependent anisotropy parameters.

4.2. $NdAl_2$ - a Kramer's Doublet Ground State System

The crystal field parameters B_4 and B_6 and the mean-field constant λ were determined in chapter 3 by analysing the exciton spectrum. Assuming that the Nd^{3+} ions can be described by the Hamiltonian (4.1), we are then in possession of all the parameters necessary to determine the bulk magnetic properties of $NdAl_2$, such as magnetization, susceptibility, and magnetic specific heat.

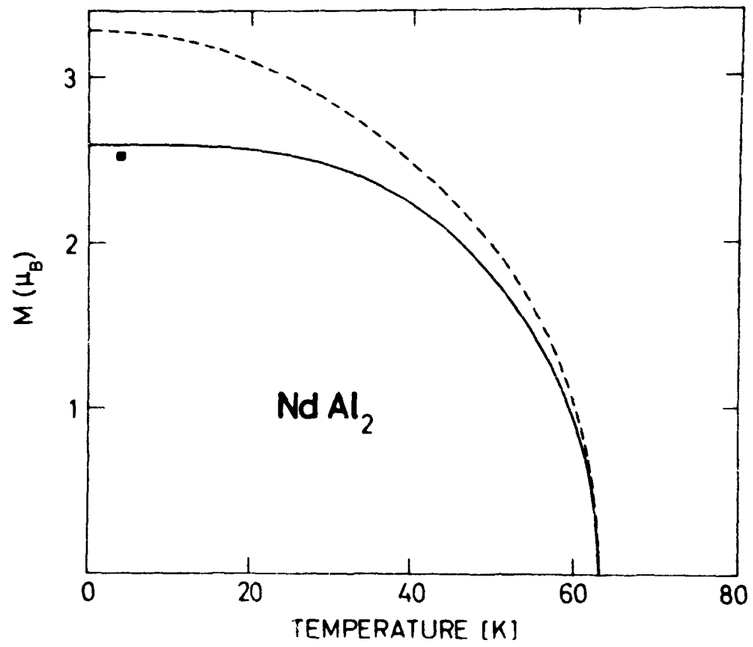

Fig. 6. The theoretical spontaneous magnetization of $NdAl_2$ in the <100> direction. The broken line is the Brillouin curve for J = 9/2. The experimental point was determined by neutron diffraction[4].

The spontaneous magnetic moment ($\vec{H}_e = 0$) is presented in figure 6 as a function of temperature. At low temperatures the exchange field admixes the excited multiplets into the Γ_6 ground state, raising the magnetic moment from the value 1.33 μ_B associated with the Γ_6 state to 2.60 μ_B. This is in agreement with the value 2.53 ± 0.1 μ_B observed by neutron diffraction[4]. The quenching of the free ion moment 3.27 μ_B can thus be explained as a pure crystal field effect. The magnetic moment was also measured as a function of temperature, but unfortunately the data were not quoted in the paper.

Theoretical single crystal magnetization curves are shown in figure 7 together with experimental points at 4.2 K. The saturation moment at 4 K determined from the magnetization measurements is

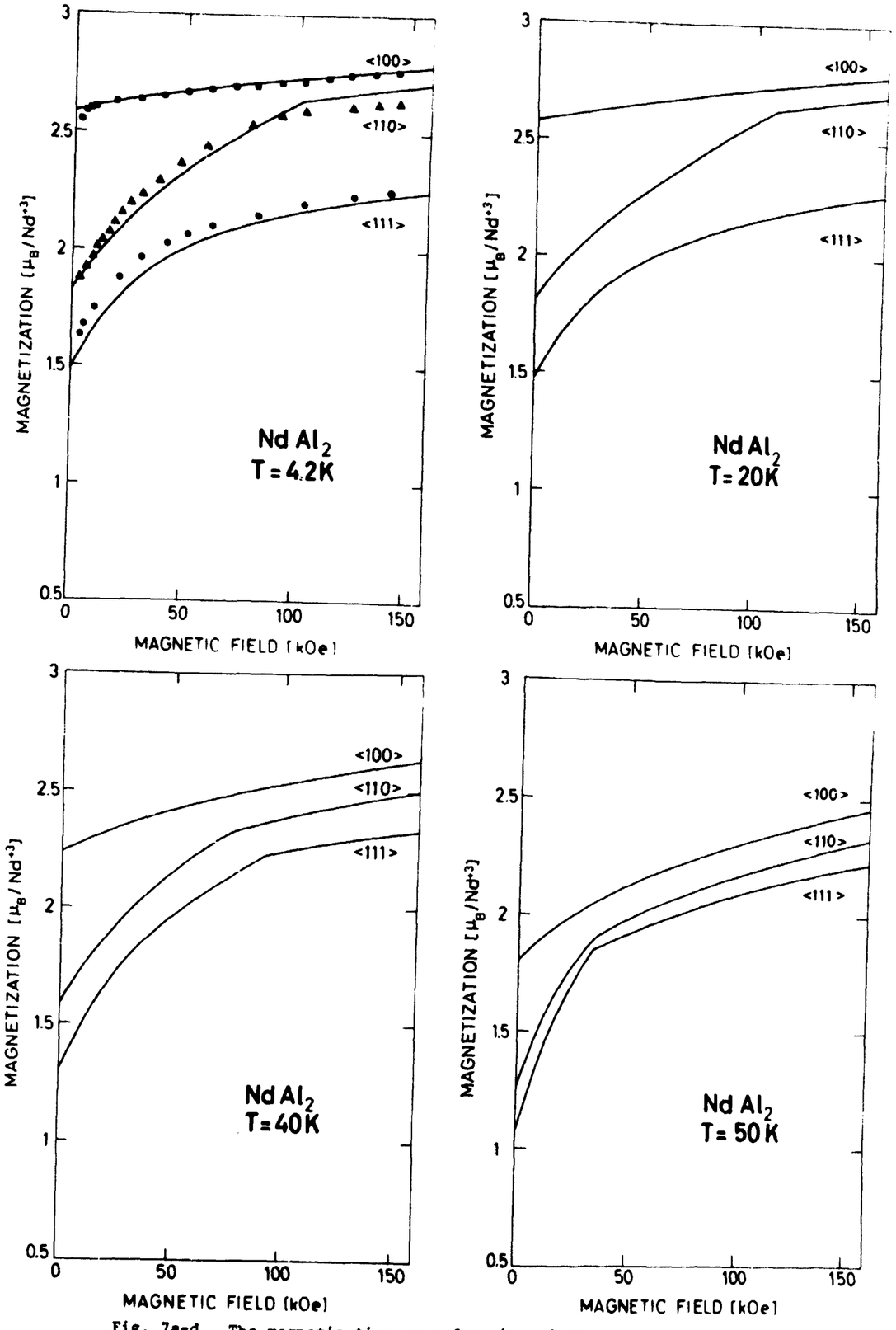

Fig. 7a-d. The magnetization as a function of the external magnetic field for $NdAl_2$ in the three main symmetry directions. The observed[35] and theoretical moments are the components along the applied magnetic field. The full curve was calculated with the parameters given in the text. The measured points have been augmented by 8% to normalize to the calculated spontaneous moment at 4 K.

2.4 μ_B[35] which is a little lower than the value 2.53 determined by neutron diffraction. To facilitate the detailed comparison with experiment, and to avoid confusing the drawing, we have normalized the experimental points to agree with the theoretical zero field magnetization at 4 K. This involves an enhancement of the observed points by 8% and brings the magnetization data in better agreement with the neutron diffraction moment. The normalized experimental points are seen to be in detailed agreement with theory. The kinks on the theoretical magnetization curves indicate the critical magnetic fields where the magnetization vector is aligned along the field. For $NdAl_2$ this alignment involves a second-order transition. At 4.2 K the kink occurs at 100 kOe. The 8% discrepancy is certainly within what could be expected from a mean-field theory without any fitting parameters, further it is well within the uncertainties associated with the determination of the crystal field parameters and the mean-field constant from the exciton experiment. The measurements thus support the crystal field parameters derived in 3.1.,the detailed behaviour of the magnetization being strongly dependent on the crystal field parameters. The present data give no justification for changing the simple crystal field model of $NdAl_2$ by introducing additional effects, such as anisotropic exchange interactions or magnetoelastic effects. It is rather surprising that these effects are not manifested in the magnetization curves.

4.3. $PrAl_2$ - a Non-magnetic-Doublet Ground State System

The crystal field parameters and the exchange constant were determined by fitting to the magnetization curves at 4.2 K (figure 10) and the temperature dependence of the spontaneous magnetization curve[33] (figure 8). We find

$$B_4 = -4.4 \times 10^{-3} \text{ meV} \qquad B_6 = -8.8 \times 10^{-5} \text{ meV}$$

$$\lambda = 161.5 \text{ kOe}/\mu_B$$

The energies and the wave functions of the crystal field levels are given in the diagram in figure 20. We note that the ground state of the Stark-splitted J-multiplet is an orbital degenerate Γ_3 doublet. The peculiar feature of this doublet is that its

degeneracy cannot be removed by a magnetic field, i.e. Γ_3 is a non-magnetic orbital doublet. $PrAl_2$ is - as far as we know - the first compound for which the ground state has been shown to be a degenerate, but non-magnetic, state. In such a system, ordering takes place via the admixing of excited states into the ground state, provided the exchange interaction exceeds a certain threshold value. This is in analogy with the "bootstrap" process occurring in singlet ground state systems[36]. However, the ground state is not a singlet state as assumed by Wallace et al.[37,38]. The critical value of λ is the value for which the susceptibility approaches infinity at T = 0; $\lambda_{crit.}$ is thus identical to the single-ion susceptibility at T = 0. Using eq. (4.17) together with (3.4) we find

$$\lambda_{crit.} = 105.6 \text{ kOe}/\mu_B$$

The actual exchange constant exceeds the critical value by a factor 1.5; hence the system is only slightly overcritical. In fig. 8 the full line is the calculated magnetic moment in the easy direction in zero magnetic field as a function of temperature. For comparison

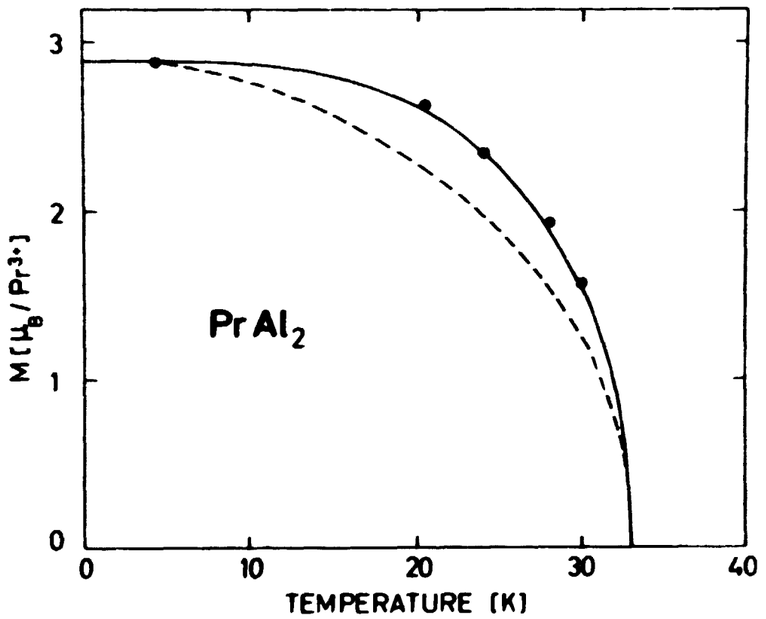

Fig. 8. Spontaneous magnetic moment of $PrAl_2$ as a function of temperature. Points: experiment[33]. Curves: theory. The parameters $B_4 = -44 \times 10^{-4}$ meV, $B_6 = -88 \times 10^{-6}$ meV, and $\lambda = 161.5$ kOe/μ_B were used. The broken line is the Brillouin curve for J = 4.

we give the Brillouin curve for J = 4 normalized to the measured zero temperature moment of 2.88 μ_B (broken line). The quenching of the free ion moment 3.2 μ_B can thus be completely understood as a crystal field effect. The theoretical magnetization curves for all measured temperatures are given in figs. 10a-10e. The corresponding field dependence of the magnetization vector at 30 K is shown in figure 9. In view of the simplicity of the theoretical model (molecular field theory, magnetostriction and eventual anisotropic exchange have been neglected), we find excellent agreement between theory and experiment. In particular we note (figure 10e) that the calculated magnetic moment in the <111> direction exhibits a small jump at 30 K which is indicated experimentally only 2 K lower for the same magnetic field (figure 10d). The jump indicates that the alignment of the magnetic moment along the magnetic field involves a first order transition (figure 9b).

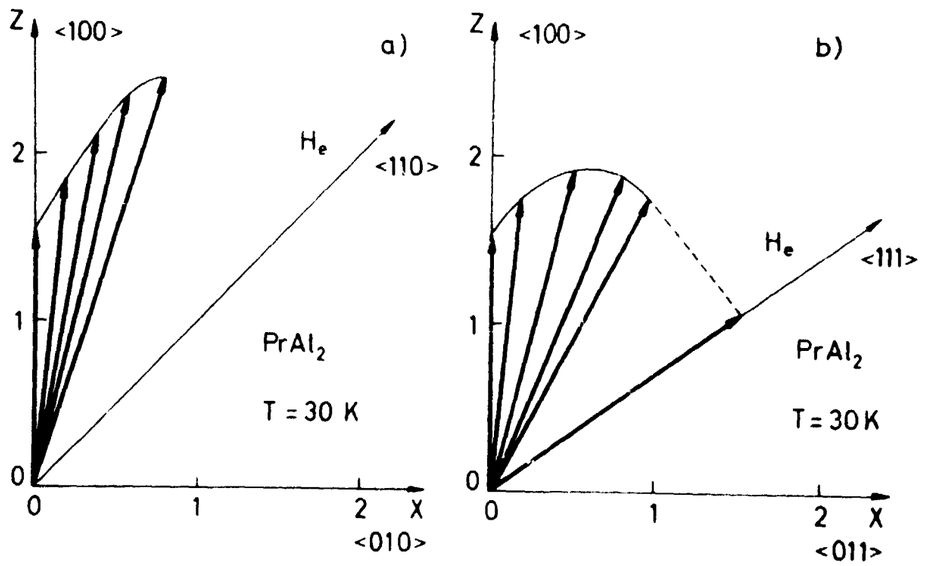

Fig. 9. The theoretical magnetization vector for $PrAl_2$ at 30 K as a function of magnetic field in high symmetry directions. a) H_e in the <110> direction. The $\vec{M}$ vectors are calculated for H_e = 0, 18, 63, 143, 280 kOe. b) H_e in the <111> direction H_e = 0, 13, 55, 97, 112 kOe. The magnetic moments are given in Bohr magnetons.

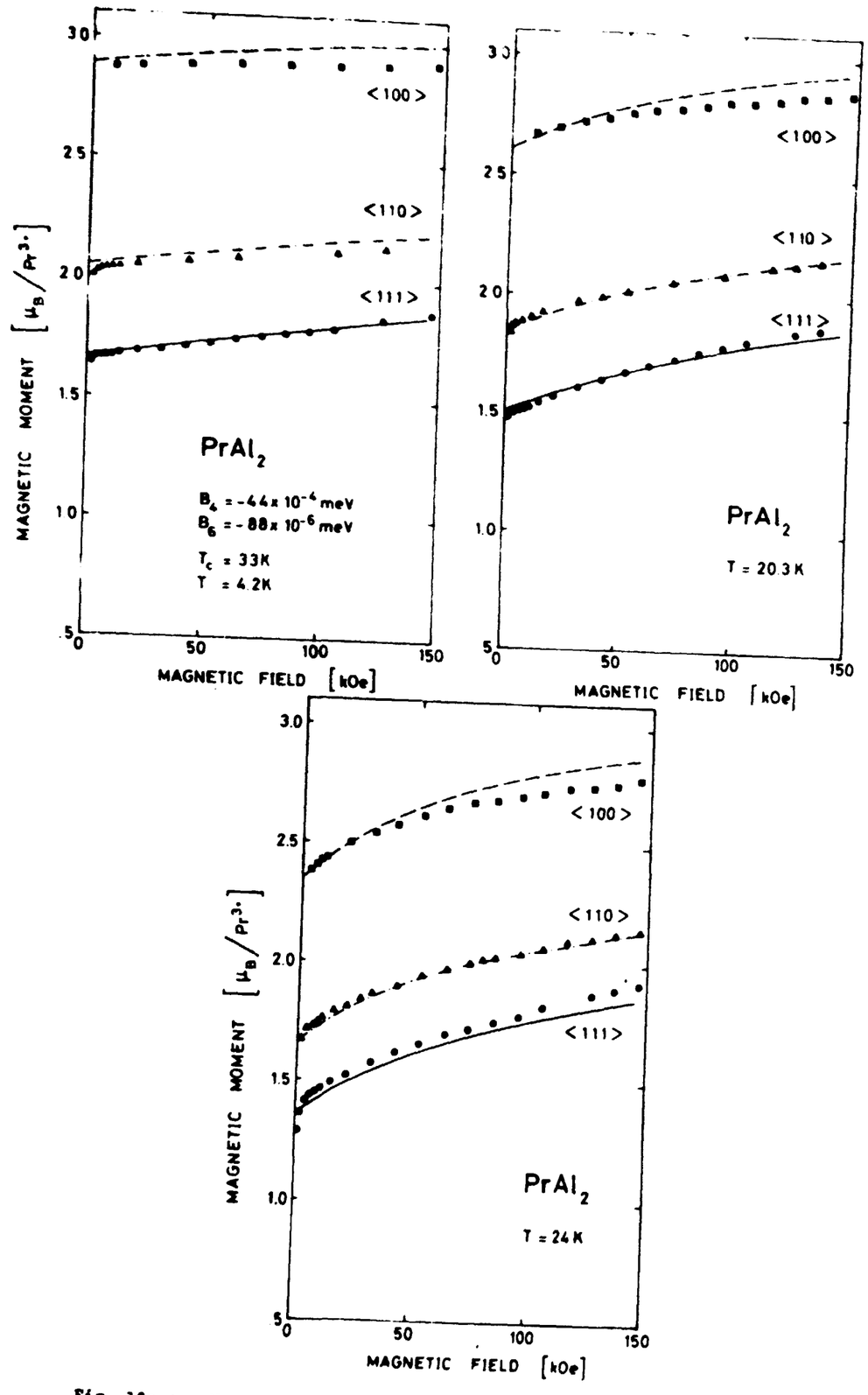

Fig. 10a-e. Magnetization in symmetry directions in $PrAl_2$ for various temperatures as a function of magnetic field. Full lines: theory. Points: experiment[33].

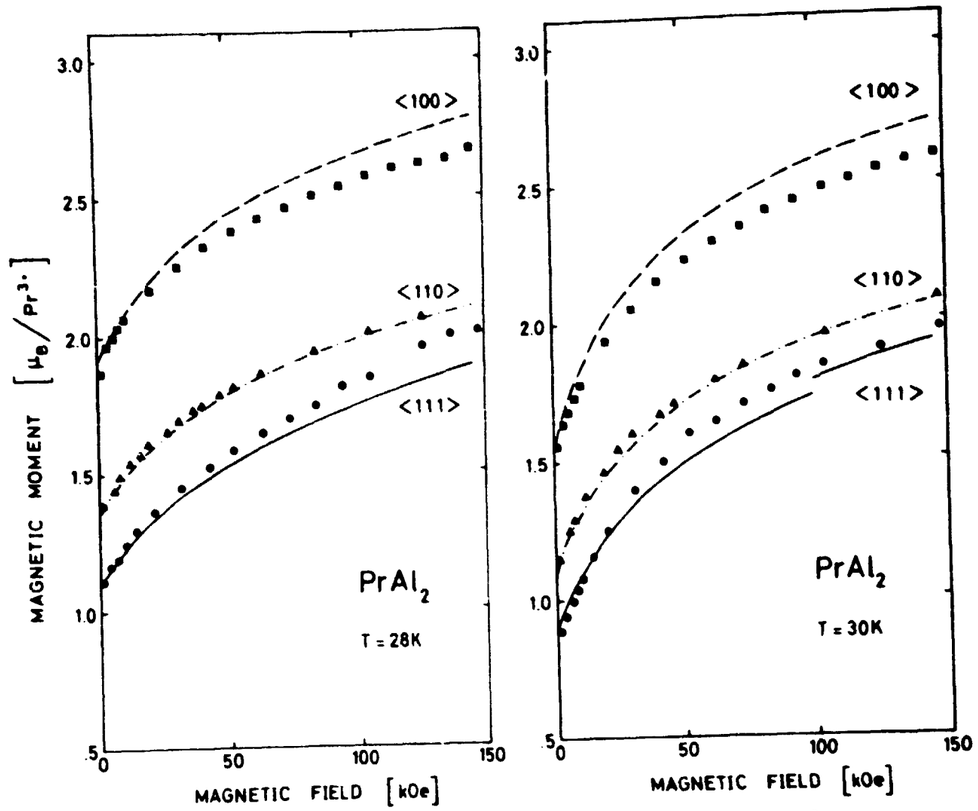

Fig. 10a-e. Magnetization in symmetry directions in $PrAl_2$ for various temperatures as a function of magnetic field. Full lines: theory. Points: experiment[33].

4.4. $TbAl_2$ - a Singlet-triplet System

The calculations on $TbAl_2$ were performed in exactly the same way as for $PrAl_2$. According to the opposite signs of the Stevens γ and β-factors[39] (see eq. (5.1.) in $TbAl_2$ and $PrAl_2$, <111> is the easy and <100> the hard direction of magnetization. The parameters

$$B_4 = 3.0 \times 10^{-4} \text{ meV} \qquad B_6 = 0.25 \times 10^{-6} \text{ meV}$$

$$\lambda = 47.5 \text{ kOe}/\mu_B$$

give the best fit to experiments[11,44,33]. These parameters are somewhat smaller than the parameters used to describe the exciton experiment. This can be due to the simplifications used in the interpretation of the magnon exciton interaction in $TbAl_2$. The two lowest crystal field states are a Γ_1 singlet ground state and a Γ_4 excited triplet state, separated by 6.2 K = 0.53 meV (figure 21). Investigations of the superconductivity in $Tb_xY_{1-x}Al_2$[40] require a non magnetic ground state and a first excited state at .4 meV. This is in agreement with the level scheme derived here

though the authors attribute other signs to B_4 and B_6. Due to the work of J.R. Cooper[41] the level scheme of Tb in $LaAl_2$ should consist of a non-magnetic ground state, Γ_3, and a magnetic first excited state, Γ_5, with 5 K level separation. This is incompatible with the present analysis. Measurements of the Schottky anomaly in the specific heat yield an energy splitting of 6 K[42]. From measurements of the thermopower anomaly[43] a splitting of 7 ± 1 K was found.

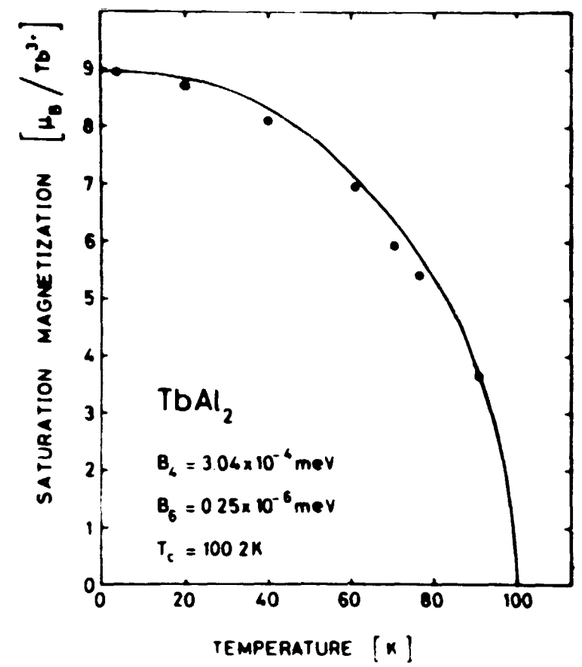

Fig. 11. Spontaneous magnetic moment of $TbAl_2$. The points were measured by Purwins et al.[44]. For the theoretical curves the parameters $B_4 = 3.04 \times 10^{-4}$ meV, $B_6 = 0.25 \times 10^{-6}$ meV and $\lambda = 47.5$ kOe/μ_B were used.

Figure 11 shows the spontaneous magnetization versus temperature. In figures 12a-g we compare the calculated magnetization curves with experiment. Again we find detailed agreement. The critical value of λ for magnetic ordering is

$$\lambda_{crit.} = 1.5 \text{ kOe}/\mu_B$$

The ratio between the actual and the critical values of λ is 32. The crystal field is thus not strong enough to produce considerable deviations from a Brillouin curve with J = 6 and a magnetic moment of 9 μ_B at zero temperature.

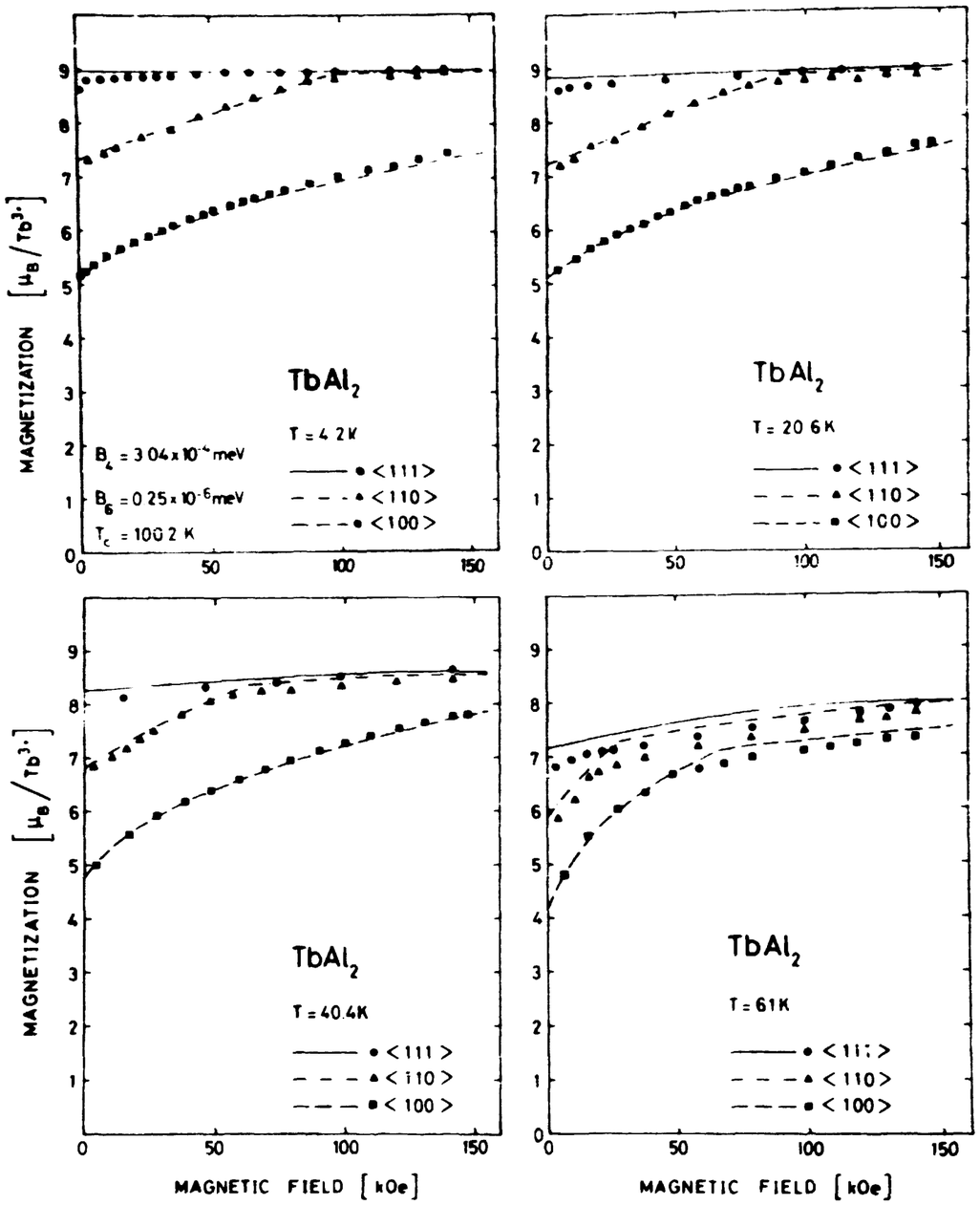

Fig. 12a-g. Magnetization in symmetry directions in $TbAl_2$ for various temperatures as a function of magnetic field. Full lines: theory. Points: experiment[11,44].

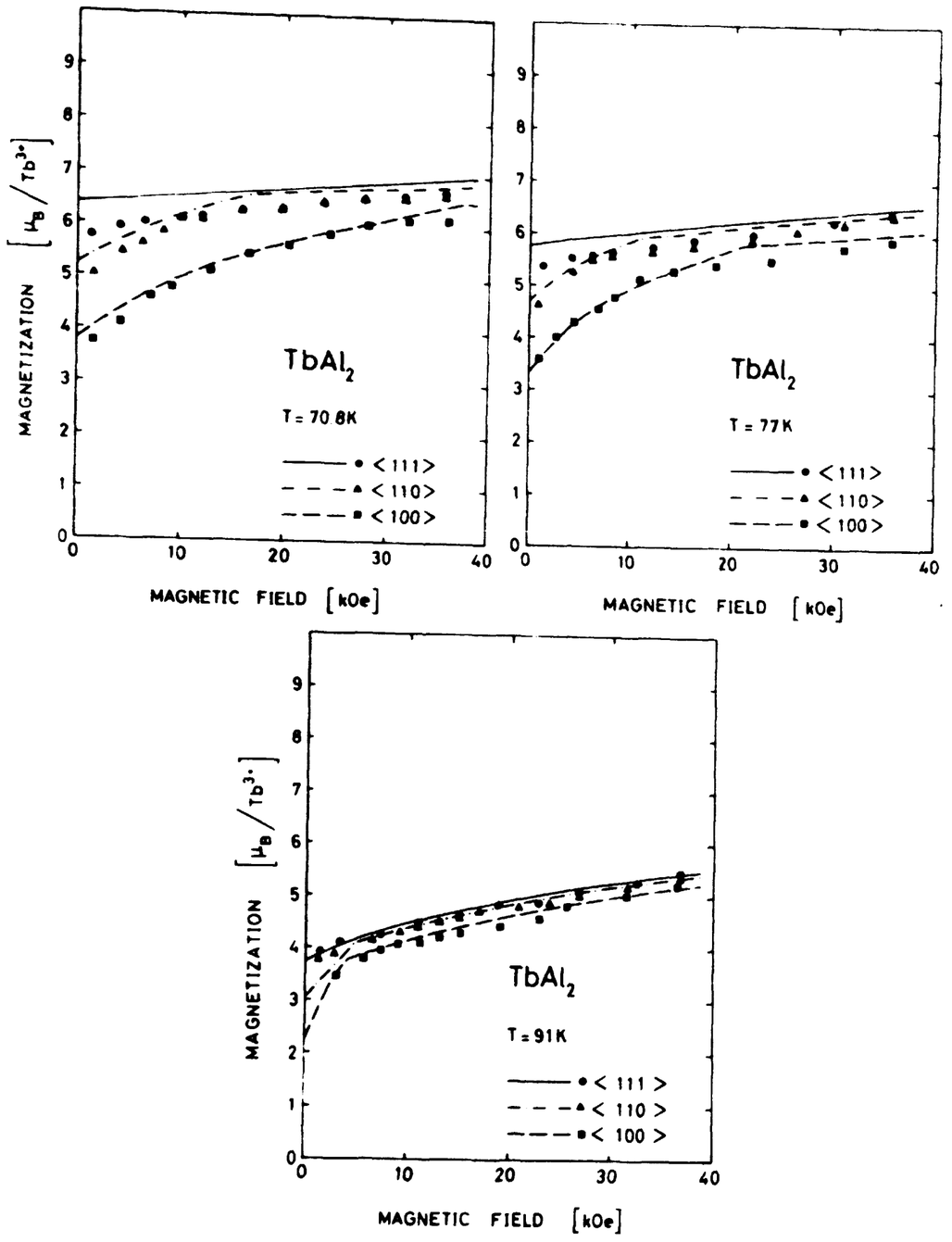

Fig. 12a-g. Magnetization in symmetry directions in $TbAl_2$ for various temperatures as a function of magnetic field. Full lines: theory. Points: experiment[11,44].

4.5. $ErAl_2$

A similar analysis of $ErAl_2$ gives the parameters

$$B_4 = 1.0 \times 10^{-4} \text{ meV}, \qquad B_6 = -1.5 \times 10^{-6} \text{ meV}.$$

The experimental[3] and theoretical magnetization curves are shown in fig. 13. The crystal field lowers the spontaneous magnetic moment at 0 K from the free ion value 9 μ_B to about 7.7 μ_B. However, neutron diffraction measurements yield a magnetic moment of 8.3 μ_B[5].

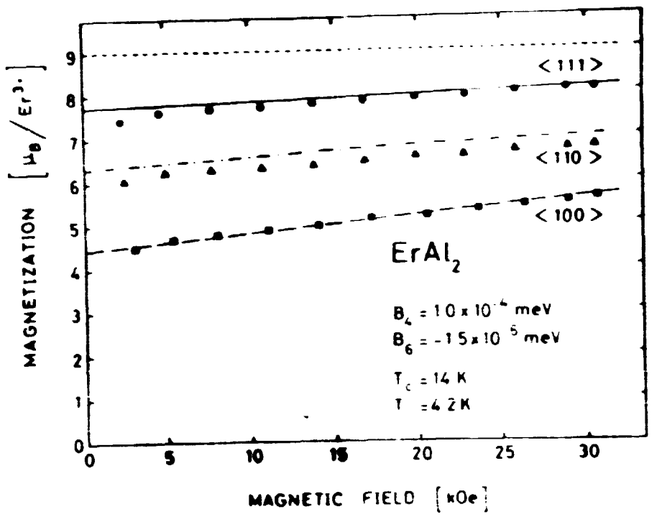

Fig. 13. Magnetization curves of $ErAl_2$. Points: experiment[3]. Curves: theory.

4.6. Heat Capacity of $NdAl_2$ and $PrAl_2$

In contrast to the very extensive work on the magnetic behaviour of the $REAl_2$ compounds, comparatively little work has been done on their heat capacities and associated thermodynamic characteristics. The work of Deenadas et al.[9] seems to be the only study of the compounds which we are considering.

The molar magnetic heat capacity C_p - within the single-ion picture - is given by the formula

$$\frac{C_p}{R} = \frac{d\langle \mathcal{H}_1 \rangle}{dT} = \frac{d}{dT} \frac{\sum_i E_i \exp(-\frac{E_i}{kT})}{\sum_i \exp(-\frac{E_i}{kT})}, \tag{4.13}$$

where R is the gas constant. In the paramagnetic regime, where the energy levels are temperature independent, the differentiation can easily be carried out:

$$\frac{C_p}{R} = \langle (\frac{\mathcal{H}_1}{kT})^2 \rangle - \langle \frac{\mathcal{H}_1}{kT} \rangle^2 . \tag{4.14}$$

In the ferromagnetic case, where the single-ion energy levels E_i are temperature dependent, C_p is calculated by differentiating through the effective field H_{MF}.

$$\begin{aligned} \frac{C_p}{R} &= \frac{d\langle \mathcal{H}_1 \rangle}{dT} = \frac{\partial \langle \mathcal{H}_1 \rangle}{\partial T} + \frac{\partial \langle \mathcal{H}_i \rangle}{\partial H_{MF}} \frac{d H_{MF}}{dT} \\ &= \frac{\partial \langle \mathcal{H}_1 \rangle}{\partial T} + \sum_i \frac{\partial \langle \mathcal{H}_1 \rangle}{\partial E_i} \frac{d E_i}{d H_{MF}} \frac{\lambda dM}{dT} . \end{aligned} \tag{4.15}$$

By carrying out the differentiations, we find that the heat capacity is

$$\begin{aligned} \frac{C_p}{R} = {} & \langle (\frac{\mathcal{H}_1}{kT})^2 \rangle - \langle \frac{\mathcal{H}_1}{kT} \rangle^2 + (\frac{1}{kT})^3 (\langle M \mathcal{H}_1 \rangle - \langle M \rangle \langle \mathcal{H}_1 \rangle)^2 \\ & \times \lambda \times (1 - \lambda \chi''_o)^{-1} . \end{aligned} \tag{4.16}$$

In the derivation of (4.16) it is strictly necessary that the non-operator term in (4.1) be included. The single-ion susceptibility parallel to the magnetization, χ''_o, is given by the formula

$$\begin{aligned} \chi_o^{\alpha\alpha} = {} & \frac{1}{kT} \frac{\sum'_{nm} |\langle n|M^\alpha|m\rangle|^2 \exp(-E_n/kT)}{\sum_n \exp(-E_n/kT)} \\ & - \frac{1}{kT} \left(\frac{\sum'_{nm} \langle n|M^\alpha|m\rangle \exp(-E_n/kT)}{\sum_n \exp(-E_n/kT)} \right)^2 \\ & + 2 \frac{\sum''_{mn} |\langle m|M^\alpha|n\rangle|^2 \frac{1}{E_m - E_n} \exp(-E_n/kT)}{\sum_n \exp(-E_n/kT)} \end{aligned} \tag{4.17}$$

where k is Boltzmann's constant. The summation $\sum'$ is carried out only over states $|m\rangle$ and $|n\rangle$ with $E_n = E_m$, whereas $\sum''$ includes all

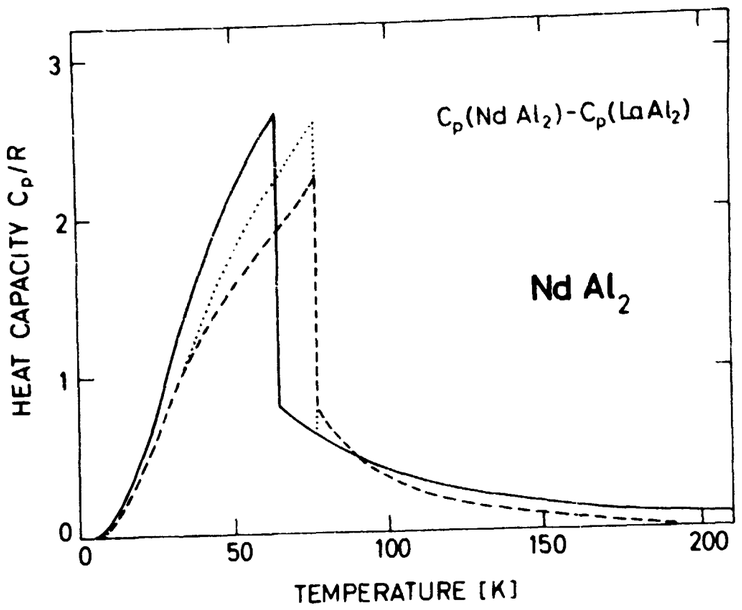

Fig. 14. The heat capacity of $NdAl_2$. Full curve: theory. Broken curve: experiment[9]. The dotted curve is calculated with the mean-field parameter readjusted to reproduce the λ-point 77.2 K determined in the experiment.

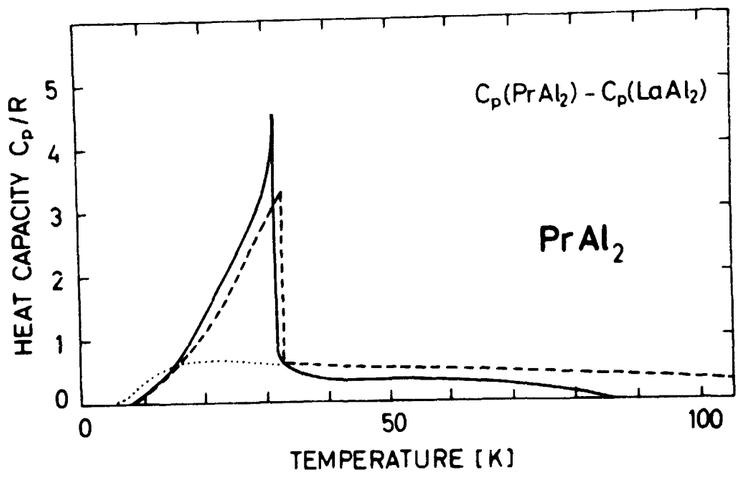

Fig. 15. The heat capacity of $PrAl_2$. Full curve: theory. Broken curve: experiment[9].

other states. For $NdAl_2$ we use the single-ion states derived in chapter 3 by analysing the exciton spectrum, and for $PrAl_2$ we use the states obtained from the analysis of the magnetization curves in 4.3. The calculated curves are shown in figs. 14 and 15 together with the magnetic heat capacities measured by Deenadas et al.[5]. The experimental curve was obtained by subtracting the heat capacity of the non-magnetic isostructural compound $LaAl_2$ from the measured heat capacities to eliminate the vibrational and electronic contributions, which can be assumed to be the same for all the compounds. The Curie temperature 77.2 K of $NdAl_2$ determined by the jump in the experimental heat capacity (the λ-point) differs significantly from the Curie temperature 65 K ± 2 K determined by neutron diffraction[4], which was used in the analysis in chapter 3 to determine the mean-field constant. When the mean-field parameter λ is readjusted to reproduce the Curie temperature 77.2 K ($\lambda = 283\ \frac{kOe}{\mu_B}$) the agreement with experiment is very satisfactory. The qualitative features of the heat capacities of the two compounds are very similar. The heat capacity shows a λ-anomaly associated with the disappearance of the ordered phase followed by a Schottky-type anomaly at higher temperatures brought about by thermal excitations of the ions into excited states. The two anomalies overlap substantially; the maximum in the heat capacity associated with the Schottky anomaly is suppressed by the onset of magnetic ordering. Only the high temperature tail is observed. The mixing of the anomalies originates from the fact that crystal field and exchange energies are comparable. The accuracy of the calculated C_p is rather surprising; the present mean-field calculation neglects both the critical phenomena around the λ-point and the specific heat associated with the magnetic excitons at low temperatures.

5. DISCUSSION

In the preceding chapters it was shown that both the bulk magnetic properties and the microscopic magnetic excitations in the $REAl_2$ compounds can be understood using a Hamiltonian containing only 2 temperature- and field-independent crystal field parameters and an isotropic exchange interaction between the RE^{+3} ions. With the two crystal field parameters and one effective

mean-field constant determined from T_c, it was possible to obtain an excellent description of the magnetization including the quenching of the magnetic moment and the anisotropy of the magnetization throughout the ordered temperature range. We emphasize that it was not necessary to introduce any temperature-dependent, phenomenological anisotropy parameters. The magnetic anisotropy is thus primarily a consequence of the effective crystal field perturbing the ground state J-manyfold of the magnetic ions. The effects of magnetostriction and anisotropic exchange interaction seem to be small in view of the success of the simplified model.

In this chapter we shall discuss and compare the crystal field parameters and the exchange interaction for the various compounds. It will be shown that the crystal field parameters show a systematic behaviour over the whole series.

5.1. Comparison of Crystal Field Parameters

Provided that the effective crystal field originates from the Coulomb interaction between the single 4f electrons and a charge distribution outside the 4f shell, the crystal field parameters can be written in the form[45]

$$B_4 = A_4 \langle r^4 \rangle \beta a^{-5},$$
$$B_6 = A_6 \langle r^6 \rangle \gamma a^{-7}, \qquad (5.1)$$

where a is the lattice parameter, β and γ are the Stevens factors[39], and $\langle r^n \rangle$ represents free ion matrix elements. This is the so-called "point charge model", although the real charge distribution need not consist of point charges on the surrounding ions. As the different compounds differ only with respect to the well-localized 4f-electrons, which probably do not influence the surroundings significantly, it seems likely that the reduced crystal field parameters A_4 and A_6 are the same for the whole isostructural Al_2 series. To test this hypothesis, we calculate A_4 and A_6 using B_4 and B_6 values derived in this work together with reliable values of other authors (table 2). For $\langle r^n \rangle$ we used non-relativistic values[46]. There may be an error of the order of 20% due to relativistic effects. The uncertainty on the crystal field parameters is generally of the same order of magnitude.

Table 2

Comparison of the crystal field parameters for $REAl_2$ compounds. Besides the parameters determined in this work, parameters obtained by other authors are included

Compound	Obtained directly from experiment B_4 10^{-4}meV	B_6 10^{-6}meV	A_4 Arbitrary units	A_6	Measured quantity	Ref.
$CeAl_2$	250	-	0.38		specific heat	9)
$PrAl_2$	-44	-88	0.64	-0.43	magnetization	
$NdAl_2$	-10	40	0.44	-0.41	mag. excitons	
$TbAl_2$	2	.2	0.30	-0.13	magnetization	44)
$TbAl_2$	3.0	.25	0.46	-0.17	magnetization	
$TbAl_2$	7.0	2.15			mag. excitons	
$ErAl_2$	1.0	-1.5	0.52	-0.69	magnetization	
$Er_{.15}Y_{.85}Al_2$	1.6	-0.60	0.71	-0.30	inelastic neutron scattering; susceptibility	
$Tm_xY_{1-x}Al_2$	3.3	2.6	0.52	-0.48	inelastic neutron scattering; susceptibility	48)
$Tm_xY_{1-x}Al_2$	3.3	2.6	0.52	-0.48	specific heat	49)

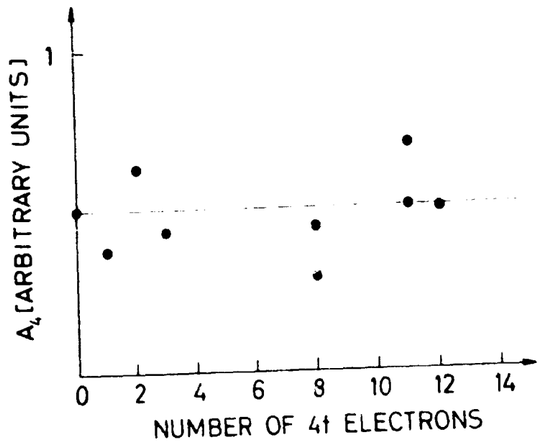

Fig. 16. The reduced crystal field parameters, A_4, for the $REAl_2$ series.

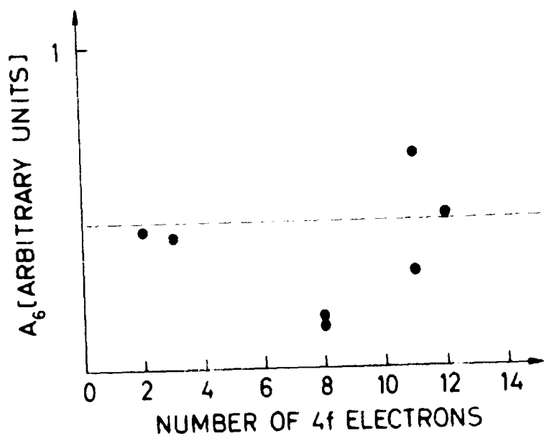

Fig. 17. The reduced crystal field parameters, A_6, for the $REAl_2$ series.

The resulting values of A_4 and A_6 are plotted in figs. 16 and 17. The points represent 9 independent measurements. The correlation between the values for the different compounds is indeed remarkable. Only the A_6 parameter for $TbAl_2$ seems to be a little too small; however, the magnetization curves are only slightly dependent on the A_6 parameters due to the small reduced matrix element γ for the Tb^{3+} ion, so that a large uncertainty must be attributed to this parameter. Thus the simple "point charge model" is valid for the $REAl_2$ compounds to a good approximation. However, we have not tried to assign specific point charges to the surrounding ions. This is in striking disagreement with the results for the diluted rare earth metals obtained by Høg and Touborg[50]; not even the signs were consistent with the point charge model. On the other hand, the simple model seems to account satisfactorily for the rare-earth group V compounds[57]. At present no explanation has been given for the fundamental difference in the nature of the effective crystal field of the diluted rare earth elements compared with the above-mentioned compounds.

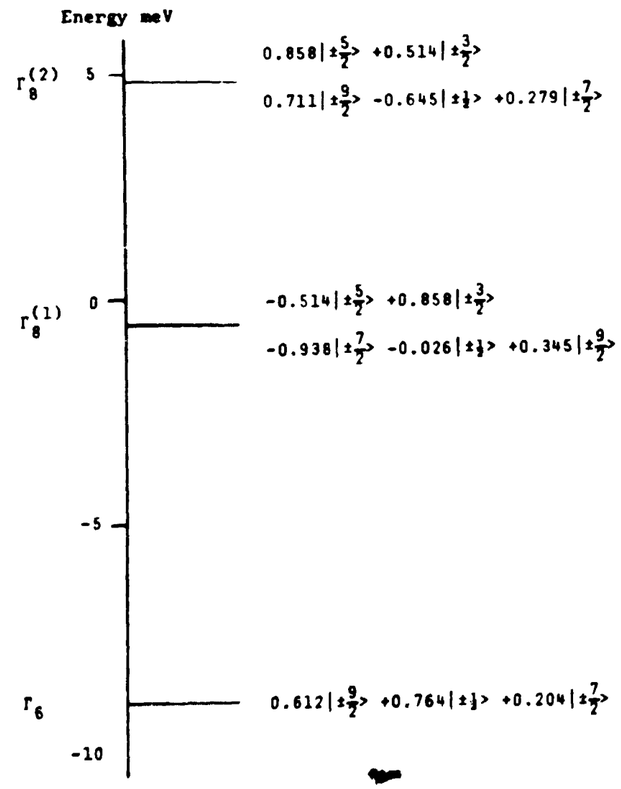

Fig. 18. Crystal field levels of $NdAl_2$

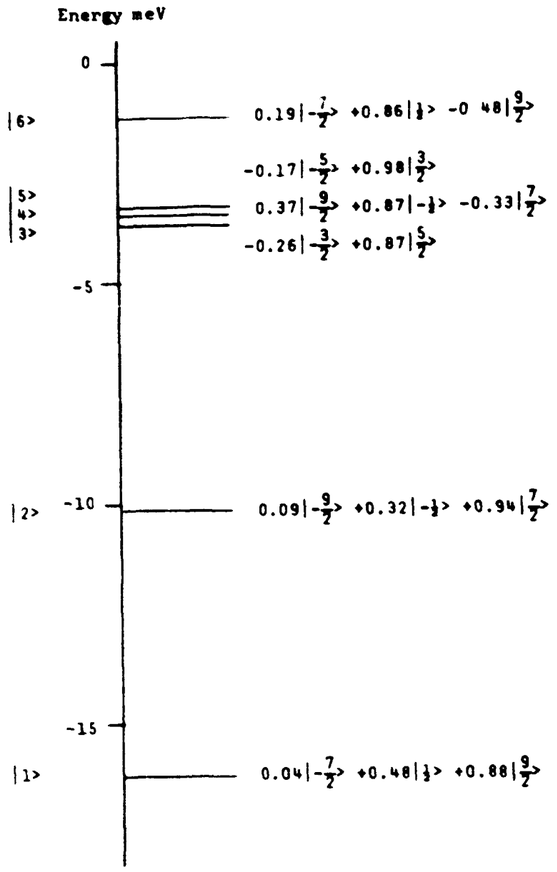

Fig. 19. Molecular field levels of $NdAl_2$ at 5 K

The $REAl_2$ system offers us three fundamentally different crystal-field-only level schemes (figs. 18, 20, 21). Besides influencing the magnetic properties, the crystal field levels play a crucial role in determining superconducting and transport properties of diluted magnetic systems[58], the conduction electron scattering on the RE-ions being strongly dependent on the crystal field wavefunctions.The non-magnetic compound $LaAl_2$ is superconducting below 3.3 K[41]. As the crystal field model seems to be valid also for $RE_xLa_{(1-x)}Al_2$ systems, the crystal field effects on the superconducting properties of such diluted systems can be calculated using the level scheme derived in this work. A systematic study of RE-ions substituted in $LaAl_2$ compounds is desirable.

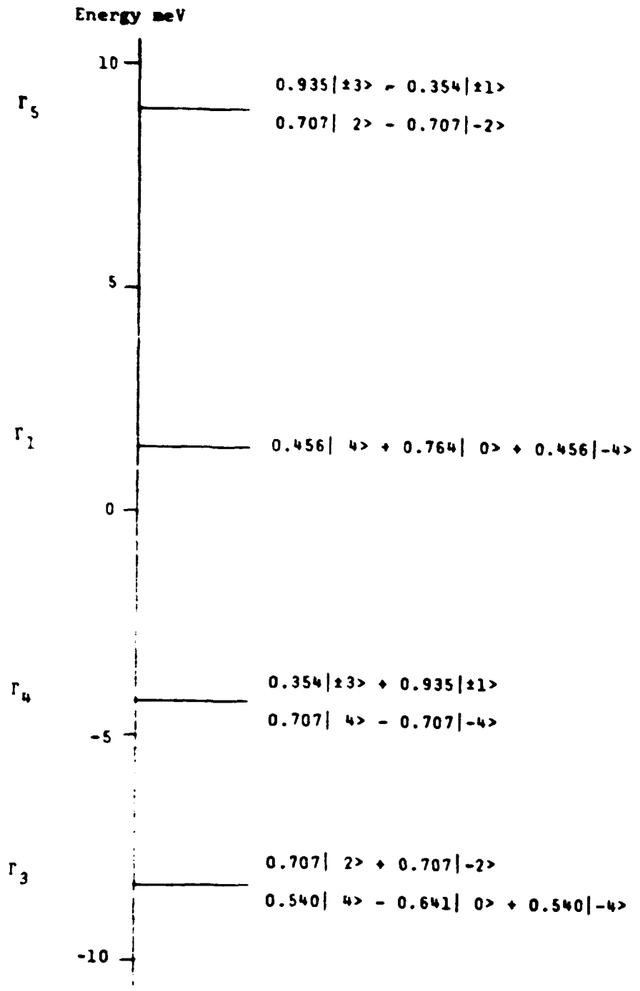

Fig. 20. Crystal field levels of $PrAl_2$

Besides the experiments quoted here, there are indeed EPR measurements on $Dy_xY_{1-x}Al_2$, $Ho_xY_{1-x}Al_2$ and $Tm_xY_{1-x}Al_2$[51] which are interpreted in terms of CEF parameters where at least one of the parameters B_4 and B_6 have reversed sign (see also section 4.4.). However, later measurements demonstrate that the EPR results are almost incompatible with the Schottky specific heat, at least in the case of $Tm_xY_{1-x}Al_2$[49]. A re-examination of J.R. Cooper's susceptibility measurements on $Tm_xLa_{1-x}Al_2$[41] allows for the parameters deduced from table 2 as well as for the parameters actually used. H.W. de Wijn et al.[56] have explained an abnormal temperature dependence of the paramagnetic Knight shift in $SmAl_2$ as a crystal field effect including excited J-levels. The spin orbit

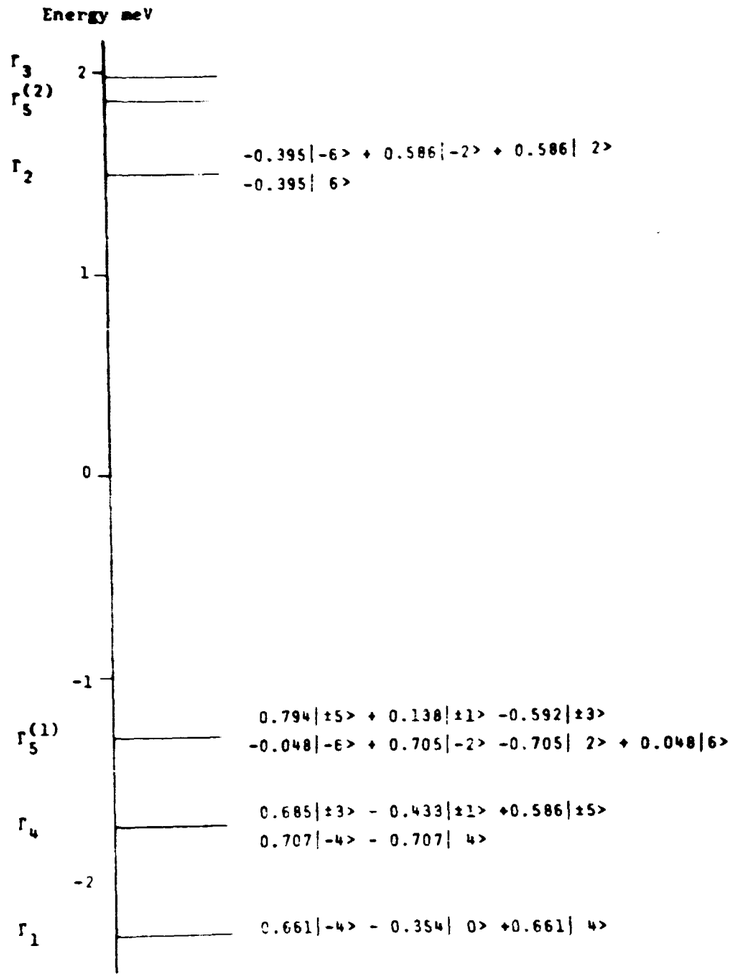

Fig. 21. Crystal field levels of $TbAl_2$

splitting is smaller for Sm compounds than for the other RE compounds. However, assuming that the scaling law (5.1.) is valid also for $SmAl_2$, the crystal field parameters used in the analysis of de Wijn are more than an order of magnitude too large.

5.2. Comparison of Exchange Parameters

Besides the crystal field parameters, the analysis yielded detailed information about the exchange interaction in $NdAl_2$. The similarity of the Fourier-transformed exchange constants $\mathcal{J}(\vec{q})$ and $\mathcal{J}'(\vec{q})$ for $NdAl_2$ and $TbAl_2$ (fig. 2) implies that the interactions are of the same nature in the two compounds. By Fourier transforming $\mathcal{J}(q)$ and $\mathcal{J}'(q)$ it has been shown[20] that for $TbAl_2$ the exchange

interaction is of long range and oscillatory, with the dominant contribution from the interaction between nearest neighbour Tb ions. The present analysis on $NdAl_2$ shows that the exchange has a similar RKKY-like behaviour in $\vec{r}$ space as anticipated in the introduction. However, it must be stressed that the exchange interaction does not scale with the de Gennes factor $(g-1)^2$, indicating that orbital effects in the two-ion interactions are important, as already pointed out by Levy[26] from an analysis of the Curie temperatures.

5.3. Conclusion

The magnetic properties of the $REAl_2$ compounds - including the magnetic excitons in $NdAl_2$ and the magnon-exciton interaction in $TbAl_2$ - can be understood using only two crystal field parameters (which are neither dependent on temperature, nor on the particular rare earth ion involved), and an isotropic RKKY-like exchange interaction. It seems justified to state that the magnetic properties of the $REAl_2$ series are now better understood than the properties of any other rare earth isostructural family. The $REAl_2$ compounds can serve as a model system for an investigation of the magnetism of rare earth intermetallic compounds.

ACKNOWLEDGMENTS

The author is much indebted to Hans-Georg Purwins for numerous invaluable discussions and to Jens Houmann for performing most of the neutron scattering measurements, without which this work would not have been possible. Furthermore, Barbara, Boucherle, and Rossignol are acknowledged for communicating as yet unpublished magnetization measurements on $NdAl_2$. Finally, thanks are due to P.A. Lindgård and J. Jensen for critically reading the manuscript.

REFERENCES

1) J.H. Wernick and S. Geller, Trans AIME 218, 866-68 (1960).

2) H.J. Williams, J.H. Wernick, E.A. Nesbitt, and R.C. Sherwood, J. Phys. Soc. Japan 17, suppl. B-1, 91-95 (1962).

3) H.-G. Purwins, Z. Physik 233, 27-36 (1970).

4) N. Nereson, C. Olsen, and G. Arnold, J. Appl. Phys. 37, 4575-80 (1966).

5) N. Nereson, C. Olsen, and G. Arnold, J. Appl. Phys. 39, 4605-09 (1968).

6) C.E. Olsen, G. Arnold, and N. Nereson, J. Appl. Phys. 38, 1395-96 (1967).

7) V. Jaccarino, B.T. Matthias, M. Peter, H. Suhl, and J.H. Wernick, Phys. Rev. Lett. 5, 251-53 (1960).

8) K.H.J. Buschow, J.F. Fast, A.M. van Diepen, and H.W. de Wijn, Phys. Stat. Sol. 24, 715-20 (1967).

9) C. Deenadas, A.W. Thompson, R.S. Craig, and W.E. Wallace, J. Phys. Chem. Solids 32, 1853-66 (1971).

10) W.M. Swift and W.E. Wallace, J. Phys. Chem. Solids 29, 2053 -61 (1968).

11) H.-G. Purwins, E. Walker, B. Barbara, and M.F. Rossignol, Phys. Lett. 45A, 427-28 (1973).

12) H.-G. Purwins, Phys. Lett. 31A, 523-24 (1970).

13) A. Abragam and B. Bleaney, Electron paramagnetic resonance of transition ions (Oxford University Press, Oxford, 1970) 864-72.

14) K.R. Lea, M.J.M. Leask, and W.P. Wolf, J. Phys. Chem. Solids 23, 1381-1405 (1962).

15) O. Rathmann, J. Als-Nielsen, P. Bak, J. Høg, and P. Touborg (1974), to be published.

16) M.A. Ruderman and C. Kittel, Phys. Rev. 96, 99-102 (1954).

17) T. Kasuya, Progr. Theor. Phys. 16, 45-57 (1956).

18) N. Kaplan, E. Dormann, K.H.J. Buschow, and D. Lebenbaum, Phys. Rev. B7, 40-49 (1973).

19) E.D. Jones and J.F. Budnick, J. Appl. Phys. 37, 1250-51 (1966).

20) W. Bührer, M. Godet, H.-G. Purwins, and E. Walker, Sol. State Commun. 13, 881-84 (1973).

21) B. Grover, Phys. Rev. 140A, 1944-51 (1965).

22) M. Godet, E. Walker, and H.-G. Purwins, J. Less-common Met. 30, 301-2 (1973).

23) W.J.L. Buyers, T.M. Holden, E.C. Svensson, R.A. Cowley, and M.T. Hutchings, J. Phys. C4, 2139-59 (1971).

24) T.M. Holden, E.C. Svensson, W.J.L. Buyers, and O. Vogt, In: Neutron Inelastic Scattering 1972, held in Grenoble, 6-10 March 1972 (IAEA, Vienna, 1972) 553-561.

25) W. Marshall and S.W. Lovesey, Theory of Thermal Neutron Scattering (Clarendon Press, Oxford, 1971) 230-52.

26) P.M. Levy, J. Appl. Phys. 41, 902-4 (1970).

27) I. Peschel, M. Klenin, and P. Fulde, J. Phys. C5, L194-96 (1972).

28) A.H. Millhouse, H.-G. Purwins, and E. Walker, Sol. State Commun. 11, 707-12 (1972).

29) E. Callen and H.B. Callen, Phys. Rev. 139, A 455-71 (1965).

30) H.-G. Purwins, J.G. Houmann, P. Bak, and E. Walker, Phys. Rev. Lett. 31, 1585-87 (1973).

31) J.G. Houmann, P. Bak, H.-G. Purwins, and E. Walker, J. Phys. C7 (1974).

32) J. Jensen and J.G. Houmann, Phys. Rev. B, to be published (1974).

33) H.-G. Purwins, E. Walker, B. Barbara, M.J. Rossignol, and P. Bak, J. Phys. C7 (1974).

34) P. Bak and P.-A. Lindgård, J. Phys. C6, 3774-84 (1973).

35) B. Barbara, J.X. Boucherl, and M.F. Rossignol, to be published (1974).

36) B.R. Cooper and Y.L. Wang, J. Appl. Phys. 40, 1344-51 (1969), Phys. Rev. 163, 444-459 (1967).

37) W.E. Wallace, Rare Earth Intermetallics (Academic Press, New York, 1973).

38) K.H. Mader, E. Segal, and W.E. Wallace, J. Phys. Chem. Solids 30, 1-12 (1968).

39) K.W.H. Stevens, Proc. Phys. Soc. London A65, 209-15 (1952).

40) G. Pepperl, E. Umlauf, A. Meyer, and J. Keller, Sol. State Commun. 14, 161-65 (1974).

41) J.R. Cooper, Sol. State Commun. 9, 1429-32 (1971).

42) H. Happel and H.E. Hoenig, Sol. State Commun. 13, 1641-43 (1973).

43) E. Umlauf, G. Pepperl, and A. Meyer, Phys. Rev. Lett. 30, 1173-75.

44) B. Barbara, M.F. Rossignol, H.-G. Purwins, and E. Walker, Phys. Stat. Sol., to appear (1974).

45) M.T. Hutchings, Sol. State Phys. 16, 227-73 (1964).

46) A.J. Freeman and R.E. Watson, In: Magretism: A Treatise on Modern Theory and Materials, Vol. 2A, Edited by G.I. Rado and H. Suhl (Academic Press, New York, 1965) 292.

47) H. Heer, A. Furrer, E. Walker, H.-G. Purwins, and J. Kjems, J. Phys. C7, 1207-13 (1974).

48) A. Furrer, W. Bührer, H. Heer, H.-G. Purwins, and E. Walker, Int. J. Magn., 4, 63-69 (1973).

49) F. Heiniger, H.-G. Purwins, and E. Walker, Phys. Lett. A, to appear (1974).

50) J. Høg and P. Touborg, Phys. Rev., to be published (1974).

51) P.A.B. Devine, W. Zingg, J.M. Moret, and C. Shaltiel, Sol. State Commun. 12, 515-18 (1973).

52) Y.Y. Hsieh and M. Blume, Phys. Rev. B6, 2684-2709 (1972).

53) D.A. Pink, ... Phys. C2, 1246-57 (1968).

54) Y.L. Wang and B.R. Cooper, Phys. Rev. 172, 539-51 (1968).

55) D.N. Zubarev, Sov. Phys. Usp. 3, 320-344 (1960).

56) P.W. de Wijn, A.M. van Diepen, and K.H.J. Buschow, Phys. Rev. B7, 524-33 (1973).

57) K.C. Turberfield, L. Passell, R.J. Birgeneau, and E. Bucher, Phys. Rev. Lett. 25, 752 (1970).
R.J. Birgeneau, E. Bucher, J.P. Maita, L. Passell, and K.C. Turberfield, Phys. Rev. B8 5345 (1973).

58) P. Fulde and T. Peschel, Adv. Phys. 89, 1-66 (1972).

APPENDIX A

Green's Function Theory of Magnetic Excitations in Systems with Arbitrary Crystal Field Levels

In this appendix a method will be presented for the study of collective excitations in a lattice of identical magnetic ions with discrete energy levels. The excitation spectrum will be calculated directly by considering the equations of motion of operators creating transitions between single-ion states. Using the double-time Green's function technique, the equations of motion will be developed in the random-phase-approximation (RPA). This theory gives a clear picture of the physical nature of the magnetic excitations in contrast to previous theories working in artificial pseudo-spin spaces[52,53]. In order to utilize familiar angular momentum operators, one sacrifices simplicity and must deal with a complicated Hamiltonian. The present theory can be extended to systems with any two-ion interactions, both in the paramagnetic and in the ordered phases without introducing essential complications.

A.1. Green's Function Theory for Magnetic Excitations in a Bravais Lattice

We consider the Hamiltonian

$$\mathcal{H} = \sum_i V_{ci} - \sum_{ij} \mathcal{J}(\vec{r}_i - \vec{r}_j)\, \vec{J}_i \cdot \vec{J}_j \qquad (A.1)$$

V_{ci} is the crystal field Hamiltonian working on the ion at site i. This term, which may conveniently be expressed as a linear combination of Steven's operators[13], gives rise to the crystal-field level splitting of the ground state J-multiplet of a rare earth ion. Furthermore, this term may include a Zeeman term from an external magnetic field. $\mathcal{J}(\vec{r}_i - \vec{r}_j)$ is the exchange integral between the ions i and j. In the ordered phase, the Hamiltonian is separated into a two-ion term and a single-ion term in the following way

$$\mathcal{H} = \mathcal{H}_0 + \mathcal{H}_1 + N\,\mathcal{J}(0)\,\langle J^z \rangle^2 \qquad (A.2)$$

$$\mathcal{H}_o = \sum_{ci} V_{ci} - 2\mathcal{J}(0)\langle J^z\rangle \sum_i J_i^z \,, \tag{A.3}$$

$$\mathcal{H}_1 \; -\sum_{ij} \mathcal{J}(\vec{r}_i-\vec{r}_j)\, \vec{j}_i\cdot\vec{j}_j \,, \tag{A.4}$$

$$\vec{j}_i = \vec{J}_i - \langle J\rangle \vec{\epsilon}_z \,. \tag{A.5}$$

$\mathcal{H}_o$ is the molecular field Hamiltonian and $\mathcal{H}_1$ is the interacting part of the Hamiltonian giving rise to dispersion of collective excitations. The statistical average $\langle J^z\rangle$ must be calculated self-consistently. $\vec{\epsilon}_z$ is a unit vector in the magnetization direction and $\mathcal{J}(\vec{q})$ is the Fourier transform of the exchange interaction. The eigenstates of the single-ion Hamiltonian $\mathcal{H}_o$ are denoted $|n\rangle_i$ with energies E_n. To proceed further we transform the total Hamiltonian into a representation where the single-ion term is diagonal, that is to say we project any operator $\hat{O}$ onto the single-ion states $|n\rangle$

$$O_i = \sum_{mn} \langle n|O_i|m\rangle (|n\rangle\langle m|)_i \,. \tag{A.6}$$

The operators $(|n\rangle\langle m|)_i$, which create transitions between the single ion states $|m\rangle_i$ and $|n\rangle_i$, are denoted a^i_{nm}. The operators $a^i_{on} = (|o\rangle\langle n|)_i$ and $a^i_{no} = (|n\rangle\langle o|)_i$, where $|o\rangle$ is the ground state, correspond to Grover's pseudo-Bose operators b_n and b_n^+ [21]. In a singlet-singlet system these operators are identical to the pseudo-spin operators introduced by Wang and Cooper[54].

We obtain:

$$\mathcal{H} = \sum_{in} E_n a^i_{nn} - \sum_{ij}\sum_{\substack{mn\\m'n'}} \mathcal{J}(\vec{r}_i-\vec{r}_j) a^i_{mn} \times a^j_{m'n'} \times \sum_\alpha \langle m|j^\alpha|n\rangle\langle m'|j^\alpha|n'\rangle \tag{A.7}$$

α denotes the cartesian coordinates. This transformation is, of course, exact. Now we set up the equations of motion of the exciton-generating operators a^i_{pr} using the simple relation

$$a^i_{pr}\, a^j_{p'r'} = (|p\rangle\langle r|)_i (|p'\rangle\langle r'|)_j = a^i_{pr'}\delta_{ij}\delta_{rp'} \,. \tag{A.8}$$

The equations turn out to be (we choose units so that $\hbar = 1$):

$$i\,\dot{a}^i_{pr} = [a^i_{pr}, \mathcal{H}] = (E_r - E_p)a^i_{pr}$$
$$-2\sum_{i'\neq i}\sum_{mnm'} \mathcal{J}(\vec{r}_{i'}-\vec{r}_i)\, a^{i'}_{mn}\, a^i_{pm'} \sum_\alpha \langle m|j^\alpha|n\rangle\langle r|j^\alpha|m'\rangle \tag{A.9}$$
$$+2\sum_{i'\neq i}\sum_{mnm'} \mathcal{J}(\vec{r}_{i'}-\vec{r}_j)\, a^{i'}_{mn}\, a^i_{m'r} \sum_\alpha \langle m|j^\alpha|n\rangle\langle m'|j^\alpha|p\rangle$$

[,] denotes the commutator.

To obtain the excitation spectrum at finite temperatures, it is convenient to introduce the retarded double-time dependent Green's functions

$$G^{ij}_{pr,p'r'}(t) = \langle\langle a^i_{pr}(t);\, a^j_{p'r'}(o)\rangle\rangle = -i\theta(t)\langle [a^i_{pr}(t),\, a^j_{p'r'}(o)]\rangle \tag{A.10}$$

as defined by Zubarev[53]. $\theta(t)$ is the unit step function. The equations of motion of the Green's functions are evaluated using (A.9)

$$(i\frac{d}{dt} - E_r + E_p)\, G^{ij}_{pr,p'r'}(t) = \delta(t)\langle [a^i_{pr},\, a^j_{p'r'}]\rangle$$
$$-2\sum_{i'\neq i}\sum_{mnm'} \mathcal{J}(\vec{r}_{i'}-\vec{r}_i)\langle\langle a^{i'}_{mn}(t)\, a^i_{pm'}(t);\, a^j_{p'r'}(o)\rangle\rangle$$
$$\times \sum_\alpha \langle m|j^\alpha|n\rangle\langle r|j^\alpha|m'\rangle \tag{A.11}$$
$$+2\sum_{i'\neq i}\sum_{mnm'} \mathcal{J}(\vec{r}_{i'}-\vec{r}_i)\langle\langle a^{i'}_{mn}(t)\, a^i_{m'r}(t);\, a^j_{p'r'}(o)\rangle\rangle$$
$$\times \sum_\alpha \langle m|j^\alpha|n\rangle\langle m'|j^\alpha|p\rangle \,.$$

For the higher order Green's functions involving operators on three different sites we apply the simplest random phase (RPA) decoupling.

$$\text{RPA: } \langle\langle a^i_{pr}(t)\, a^{i'}_{p'r'}(t);\, a^{i''}_{p''r''}(o)\rangle\rangle$$
$$= \langle a_{pr}\rangle\langle\langle a^{i'}_{p'r'}(t);\, a^{i''}_{p''r''}(o)\rangle\rangle \tag{A.12}$$
$$+ \langle a_{p'r'}\rangle\langle\langle a^i_{pr}(t);\, a^{i''}_{p''r''}(o)\rangle\rangle \,.$$

The thermal averages $\langle a_{pr} \rangle$ must in principle be determined in a self-consistent way. However, to facilitate the calculations we insert the molecular-field averages calculated from the single-ion Hamiltonian $\mathcal{H}_1$:

$$\langle a_{pr} \rangle = \langle a_{pp} \rangle \delta_{pr} = n_p \delta_{pr} \tag{A.13}$$

n_p is the occupation number of level p. According to (A.5) we have

$$\sum_m \langle a_{mm} \rangle \langle m|j^\alpha|m \rangle = \langle j^\alpha \rangle = 0 \ . \tag{A.14}$$

The equations turn out to be

$$\begin{aligned} &(i\frac{d}{dt} - E_r + E_p)\ G^{ij}_{pr,p'r'}(t) \\ &+2 \sum_{i'} \sum_{mn} \gamma(\vec{r}_{i'} - \vec{r}_i)(n_p - n_r) \sum_\alpha \langle m|j^\alpha|n \rangle \langle r|j^\alpha|p \rangle\ G^{i'j}_{mn,p'r'}(t) \\ &= \delta(t)\ \delta_{ij}\ (n_p - n_r)\ \delta_{pr'}\ \delta_{rp'} \ . \end{aligned} \tag{A.15}$$

Because of time and translational invariance in a simple Bravais lattice, we can Fourier transform our Green's functions with respect to time and space:

$$G_{pr,p'r'}(\vec{q},\omega) = \frac{1}{2\pi} \sum_j \int_{-\infty}^{\infty} G^{ij}_{pr,p'r'}(t)\ \exp(i\vec{q}\cdot(\vec{r}_i - \vec{r}_j) + i\omega t)dt \tag{A.16}$$

$$\gamma(q) = \sum_j \gamma(r_i - r_j)\ \exp(-i\vec{q}\cdot(\vec{r}_i - \vec{r}_j)). \tag{A.17}$$

The doubly Fourier-transformed equations of motion are

$$\boxed{\begin{aligned} &G_{pr,p'r'}(\vec{q},\omega)(E_r - E_p - \omega) \\ &-\sum_{mn} G_{mn,p'r'}(\vec{q},\omega)(n_p - n_r) \times 2\gamma(\vec{q}) \sum_\alpha \langle m|j^\alpha|n \rangle \langle r|j^\alpha|p \rangle \\ &= \frac{-1}{2\pi}\ (n_p - n_r)\ \delta_{pr'}\delta_{rp'} \end{aligned}} \tag{A.18}$$

This is a linear system of equations of order D^2, where D is the degeneracy of the ground state J-multiplet. The frequencies of the excitations are the poles of the Green's functions, which are

identical to the roots of the determinant of the system of equations for fixed values of p' and r'. The roots of the diagonal elements of the characteristic matrix

$$\omega_{diag.}(\vec{q}) = E_r - E_p - 2(n_p - n_r)\gamma(\vec{q}) \sum_\alpha |\langle r|j^\alpha|p \rangle|^2$$

are the so-called non-interacting excitation frequencies. For a simple ferromagnet this term yields the low-temperature spinwave theory, if $|r\rangle$ and $|p\rangle$ are chosen as the two lower states. The off-diagonal elements due to two-ion interactions give rise to perturbations of the non-interacting energies. According to general perturbation theory, the energyshifts are largest, when the corresponding diagonal coefficients approach each other. This effect can thus be described as a resonance (or interaction) between two exciton modes.

The determinant is independent of p' and r', such that the excitation frequences are unequivocally determined. The correlation functions $\langle a_{p'r'} a_{pr} \rangle_q$ involving two a-operators can be calculated from the residues of the poles ω_p of the Green's functions $G_{pr,p'r'}(\vec{q},\omega)$ by a simple algorithm (Zubarev):

$$\langle a_{p'r'} a_{pr} \rangle_q = 2\pi \sum_{\omega_p} \mathrm{Res}(G_{pr,p'r'}(\vec{q},\omega)) \frac{1}{\exp(\omega_p \beta) - 1} \tag{A.19}$$

$\beta = \frac{1}{kT}$, where k is Boltzmann's constant. Any two-ion operator is easily expressible in terms of the a-operators, so that the formalism allows us to calculate any two-ion correlation function by Fourier transforming equations of the form (A.19).

However, the calculation of single-ion averages $\langle a_{pr} \rangle$, which according to (A.12) are necessary to carry out a fully self-consistent RPA calculation and avoid insertion of molecular-field averages, suffers severely from the fact that there is no unique way to express these averages in terms of the Green's functions. In principle $\langle a_{pr} \rangle$ can be written as any of the averages $\langle a_{pi} a_{ir} \rangle$ which may be determined from (A.19), without any restrictions on i. At low temperatures we suggest the relation

$$\langle a_{pp} \rangle = \langle a_{po} a_{op} \rangle = \frac{1}{N} \sum_q \langle a_{po} a_{op} \rangle_q \ . \tag{A.20}$$

This choice makes the contribution from the excitations to the low temperature magnetization identical to the magnetization ob-

tained from Grover's theory, or a low temperature spinwave theory.

The complex frequency dependent susceptibility can be expressed by the Green's functions:

$$\chi^{\alpha\beta}(\vec{q},\omega) = 2\pi\, i\, \text{F.T.}\theta(t)\langle[J_i^{\alpha}(t),\, J_j{}^{\beta}(0)]\rangle$$

$$= 2\pi\, i\, \text{F.T.}\theta(t) \sum_{\substack{pr \\ p'r'}} \langle[a_{pr}^{i}(t),\, a_{p'r'}^{j}(0)]\rangle \qquad \text{(A.21)}$$

$$\times \sum_{\alpha} \langle p|J^{\alpha}|r\rangle\langle p'|J^{\beta}|r'\rangle$$

$$= -2\pi \sum_{\substack{pr \\ p'r'}} G_{pr,p'r'}(\vec{q},\omega) \sum_{\alpha} \langle p|J^{\alpha}|r\rangle\langle p'|J^{\beta}|r'\rangle\ .$$

F.T. denotes the Fourier transformation with respect to time and lattice as defined by (A.16). By insertion in (A.18) we obtain

$$\chi^{\alpha\beta}(\vec{q},\omega) = \chi_o^{\alpha\beta}(\omega) + 2\gamma(\vec{q}) \sum_{\gamma} \chi_o^{\alpha\gamma}\, \chi^{\gamma\beta}(\vec{q},\omega)$$

or

$$\bar{\bar{\chi}}(\vec{q},\omega) = \bar{\bar{\chi}}_o(\omega) + 2\gamma(\vec{q})\, \bar{\bar{\chi}}_o(\omega)\cdot\bar{\bar{\chi}}(\vec{q},\omega) \qquad \text{(A.22)}$$

where

$$\chi_o^{\alpha\beta}(\omega) = \sum_{pr} \frac{\langle p|J^{\alpha}|r\rangle\langle r|J^{\beta}|p\rangle(n_p-n_r)}{E_r-E_p-\omega} \qquad \text{(A.23)}$$

$\bar{\bar{\chi}}_o$ is the single-ion susceptibility tensor. Equation (A.22) is the usual molecular-field equation to determine the complex susceptibility. The excitations found from (A.18) are thus in agreement with the excitations calculated by the method of Peschel et al.[27].

For a neutron scattering experiment it is important to know the strength of the different lines. The cross section can be expressed as the imaginary part of the dynamic susceptibility[25] using the fluctuation-dissipation theorem

$$\frac{d^2\sigma}{d\Omega d\omega}(\vec{q},\omega) \sim \frac{1}{1-\exp(-\beta\omega)} \sum_{\alpha\beta} (\delta_{\alpha\beta}-\hat{q}^{\alpha}\hat{q}^{\beta})\, \text{Im}\chi^{\alpha\beta}(\vec{q},\omega). \qquad \text{(A.24)}$$

A.2. Excitations in Systems with Two Magnetic Ions per Unit Cell

In the $REAl_2$ compounds there are two magnetic ions per unit cell, situated at two interpenetrating cubic face centered lattices (fig. 1). To calculate the excitation spectrum, we insert the following Fourier transforms in (A.15):

$$G_{pr,p'r'}(\vec{q},\omega) = \frac{1}{2\pi} \sum_{j} \int_{-\infty}^{\infty} G_{pr,p'r'}^{ij}(t)\exp(i\vec{q}\cdot(\vec{r}_i-\vec{r}_j)+ i\omega t)dt$$

$$G'_{pr,p'r'}(\vec{q},\omega) = \frac{1}{2\pi} \sum_{j'} \int_{-\infty}^{\infty} G_{pr,p'r'}^{ij'}(t)\exp(i\vec{q}\cdot(\vec{r}_i-\vec{r}_{j'})+i\omega t)dt$$

$$\gamma(q) = \sum_{j} \gamma(\vec{r}_i-\vec{r}_j)\exp(-i\vec{q}\cdot(\vec{r}_i-\vec{r}_j) \qquad \text{(A.25)}$$

$$\gamma'(q) = \sum_{j'} \gamma(\vec{r}_i-\vec{r}_{j'})\exp(-i\vec{q}\cdot(\vec{r}_i-\vec{r}_{j'})$$

where i and j are situated at the same sub-lattice and i and j' at opposite sub-lattices. For $\gamma(\vec{q})$ and $\gamma'(q)$ the following symmetry relations hold:

$$\gamma(\vec{q}) = \gamma(-\vec{q}), \qquad \gamma'(\vec{q}) = \gamma'(-\vec{q}) = |\gamma'(\vec{q})|\, \exp i\phi \qquad \text{(A.26)}$$

The equations of the Green's functions become

$$G_{pr,p'r'}(\vec{q},\omega)(E_r-E_p-\omega) \qquad \text{(A.27)}$$

$$- \sum_{mn} 2\{\gamma(\vec{q})G_{mn,p'r'}(\vec{q},\omega) + \gamma'(\vec{q})\, G'_{mn,p'r'}(\vec{q},\omega)\}$$

$$\times(n_p-n_r)\sum_{\alpha} \langle m|j^{\alpha}|n\rangle\langle r|j^{\alpha}|p\rangle$$

$$= -\frac{1}{2\pi}(n_p-n_r)\delta_{pr'}\delta_{p'r}$$

$$G'_{pr,p'r'}(\vec{q},\omega)(E_r-E_p-\omega) \qquad (A.28)$$

$$- \sum_{mn} 2\left\{\gamma(\vec{q})G'_{mn,p'r'}(\vec{q},\omega) + \gamma^*(\vec{q})G_{mn,p'r'}(\vec{q},\omega)\right\}$$

$$\times (n_p-n_r)\sum_\alpha \langle m|j^\alpha|n\rangle\langle r|j^\alpha|p\rangle$$

$$= 0.$$

Instead of the Green's functions $G_{pr,p'r'}(\vec{q},\omega)$ and $G'_{pr,p'r'}(\vec{q},\omega)$ we introduce the linear combinations

$$G^{ac}_{pr,p'r'}(\vec{q},\omega) = G_{pr,p'r'}(\vec{q},\omega) + G'_{pr,p'r'}(\vec{q},\omega)\exp(i\phi) \qquad (A.29)$$

$$G^{opt}_{pr,p'r'}(\vec{q},\omega) = G_{pr,p'r'}(\vec{q},\omega) - G'_{pr,p'r'}(\vec{q},\omega)\exp(i\phi).$$

The equations for the new Green's functions are

$$G^{ac}_{pr,p'r'}(\vec{q},\omega)(E_r-E_p-\omega) \qquad (A.30)$$

$$- \sum_{mn} G^{ac}_{mn,p'r'}(\vec{q},\omega)(n_p-n_r)\times 2(\gamma(\vec{q})\pm|\gamma'(q)|)\sum_\alpha \langle m|j^\alpha|n\rangle\langle r|j^\alpha|p\rangle$$

$$= \frac{-1}{2\pi}(n_p-n_r)\delta_{p'r}\delta_{pr'}$$

In this way we have separated the excitations into acoustic and optical modes determined by $\gamma(\vec{q})+|\gamma'(\vec{q})|$ and $\gamma(\vec{q})-|\gamma'(\vec{q})|$ respectively. The equations which determine the energies when there are two magnetic ions per unit cell are thus identical to the equations for one magnetic ion per unit cell, provided the

proper combination of $\gamma(\vec{q})$ and $\gamma'(\vec{q})$ is inserted instead of $\gamma(\vec{q})$.

Following Marshall and Lovesey[25] the neutron scattering cross-section is proportional to the imaginary part of the susceptibility $\bar{\chi}^{\alpha\beta}(\vec{\kappa},\omega)$ defined by

$$\bar{\chi}^{\alpha\beta}(\vec{\kappa},\omega) = 2\chi^{\alpha\beta}(\vec{\kappa},\omega) + \chi'^{\alpha\beta}(\vec{\kappa},\omega) + \chi'^{\alpha\beta}(-\vec{\kappa},\omega) \qquad (A.31)$$

$\chi^{\alpha\beta}(\vec{\kappa},\omega)$ is the Fourier-transformed susceptibility within one sub-lattice and $\chi'^{\alpha\beta}(\vec{\kappa},\omega)$ is the Fourier-transformed susceptibility between the two lattices. When $\vec{\kappa}$ is outside the first Brillouin zone we have

$$\vec{\kappa} = \vec{q} + \vec{\tau} \qquad (A.32)$$

$$\chi'^{\alpha\beta}(\vec{\kappa},\omega) = \chi'^{\alpha\beta}(\vec{q},\omega)\exp(i\vec{\rho}\cdot\vec{\tau}) \qquad (A.33)$$

$$\chi^{\alpha\beta}(\vec{\kappa},\omega) = \chi^{\alpha\beta}(\vec{q},\omega) \qquad (A.34)$$

where $\vec{q}$ is in the first Brillouin zone and $\vec{\rho}$ is the vector joining an ion in one sublattice to its nearest neighbour in the other subiattice. $\vec{\tau}$ is the corresponding reciprocal lattice vector.

In analogy with (A.29) we introduce the susceptibilities

$$\chi^{\alpha\beta,ac}_{opt}(\vec{q},\omega) = \chi^{\alpha\beta}(\vec{q},\omega) \pm \chi'^{\alpha\beta}(\vec{q},\omega)\exp(i\phi) \qquad (A.35)$$

$$= -2\pi \sum_{pr,p'r'} G^{ac}_{opt\,pr,p'r'}(\vec{q},\omega)\langle p|J^\alpha|r\rangle\langle p'|J^\beta|r\rangle$$

Hence the susceptibilities $\chi^{\alpha\beta,\underline{ac}}_{\underline{opt}}(\vec{q},\omega)$ can be calculated by equations similar to (A.22).

From equations (A.31) - (A.33) we get:

$$\bar{\chi}^{\alpha\beta}(\vec{\kappa},\omega) = \chi^{ac,\alpha\beta}(\vec{q},\omega)(1+\cos\phi') + \chi^{opt,\alpha\beta}(\vec{q},\omega)(1-\cos\phi') \tag{A.36}$$

$$\cos\phi' = \cos(\phi+\vec{\tau}\cdot\vec{\rho}) \tag{A.37}$$

The resulting formula for the cross section is

$$\frac{d^2\sigma}{d\Omega d\omega}(\vec{\kappa},\omega) \sim \frac{1}{1-\exp(-\beta\omega)} \sum_{\alpha\beta} (\delta_{\alpha\beta} - \vec{\kappa}^{\alpha}\vec{\kappa}^{\beta}) \times \mathrm{Im}\left[\chi^{ac,\alpha\beta}(\vec{q},\omega)(1+\cos\phi') + \chi^{opt,\alpha\beta}(\vec{q},\omega)(1-\cos\phi')\right] \tag{A.38}$$

The neutron cross-section can thus be expressed by equations identical to equation (A.24) if the magnetic structure factor $(1\pm\cos\phi')$ is taken into account.

This factor is responsible for the vanishing of the neutron cross section in certain high-symmetry directions in $NdAl_2$ and $TbAl_2$. It is because of this factor that we are able to distinguish between optical and acoustic branches in the experimental neutron scattering spectrum.

ISBN 87 550 027